Design and Validation of a Dynamic Knee Injury Simulator

by

Karla Cassidy

A thesis
presented to the University of Waterloo
in fulfillment of the
thesis requirement for the degree of
Master of Applied Science
in
Mechanical Engineering

Waterloo, Ontario, Canada, 2009

I hereby declare that I am the sole author of this thesis. This is a true copy of the thesis, including any required final revisions, as accepted by my examiners.

I understand that my thesis may be made electronically available to the public.

Abstract

The knee is one of the most complex joints in the body, relying entirely on ligaments and muscles for stabilization. With the rise in people participating in sports, including a significant increase in female athletes, the prevalence of anterior cruciate ligament (ACL) injuries is very evident. With recent research showing that ACL injuries lead to osteoarthritis 10-20 years after the injury, determining the cause of these injuries to be able to prevent them is crucial.

To date, both in-vivo and in-vitro techniques have been used to analyze the influences of the ACL injury including neuromuscular, anatomical, and kinematic. In-vivo techniques used to investigate knee kinematics is limited by the inability to take real ACL strain measurements while in-vitro techniques used to investigate anatomical considerations is limited by the inability to apply true muscular and kinematic forces.

The purpose of the present thesis is to show the design and validation of a dynamic knee injury simulator. The simulator puts a cadaver knee, original ligaments and patellar tendon still attached, through motions which put the ACL at a high-risk of injury with realistic influence of muscles. The muscular influences are applied with actuators pulling the same force profiles as natural muscles. To get realistic muscle profiles, Anybody Software is used. Anybody Software is a modeling software which puts a skeletal system through prescribed motions and using an optimization algorithm calculates the muscle force profile. The motion of the knee in the sagittal plane is simulated with actuators.

The simulator consists of four actuators which are used in force control mode to add the muscle influence to the knee. Another two belt actuators are used for the joint motions, one each for the hip and ankle. The hip will move along the resultant Z motion and the ankle will move along the resultant Y motion. Simple gait is used for initial validation, the actuators chosen have speed and force capabilities for high-risk motions.

The gait was successfully simulated and muscle force versus time profile tracked the input well. The regression coefficient study shows very good comparison. The hamstring muscle group is the only one which does not show very good comparison however this is only due to the jumpy nature of the hamstring profile. The ACL strain fell within a similar range to published gait ACL strain data. The validation was successful, and with greater available force and speeds in the actuators, showing the use of this simulator during high-risk motions is possible.

Acknowledgements

Dedication

I would like to dedicate this thesis to all those this simulator will help in the future.

Contents

List of Tables

List of Figures

Chapter 1

Introduction

Biomechanics is a very useful field for both sport enhancement and sport safety. It is the study of biological systems from a mechanical perspective which falls under both Kinesiology and Sports Medicine umbrellas [52]. With millions of people playing sports all over the world there has been a rise in the concern for safety of the athletes. Knee injuries are extremely common. Approximately 3 million people injure their knee each year in the US, with about 1 million occurring in sports [12]. Knee injuries can drastically affect an athlete's training and performance, even as much as end their athletic career. Anterior Cruciate Ligament (ACL) injuries are among the most common knee injuries seen in sports. They are extremely unpredictable and the number of occurrences is increasing drastically. As of yet their cause is unknown and can only be speculated. The purpose of this thesis is to create a dynamic knee simulator which can accurately combine all aspects to find the reasons for ACL injuries; neuromuscular, soft tissue, and body kinematics.

1.1 Knee Anatomy

1.1.1 The Joint

The knee joint is the largest and most complex diarthrosis, i.e. freely mobile joint, in the human body [22]. The knee consists of two articulating joints; the tibiofemoral joint and the patellofemoral joint, see figure 1.1. The tibiofemoral joint exists between the femur and tibia condyles, and the patellofemoral joint exists between the patella and the patellar surface on the femur [22].

The femur and tibia are the two largest weight bearing bones in the skeletal system, and all the body's weight and ground reaction forces pass through them. The condyles at the distal end of the femur are an oval shaped surface which articulate with the flat surface of the proximal tibia condyles [22]. There are no bony structures to prevent the anterior/posterior, medial/lateral, or separation motions of the surfaces. The joint relies heavily on passive and active stabilization
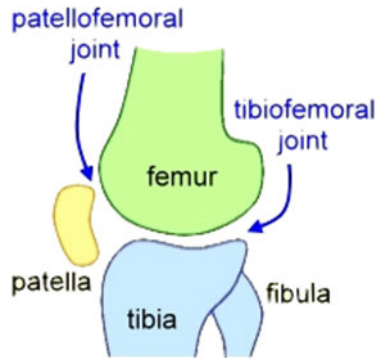
Figure 1.1: Medial View depicting Tibiofemoral and Patellofemoral Joints

for full function and stability. From these stabilizers the knee is primarily capable of flexion/extention however slight rotation and lateral gliding exists during motion causing a varying center of rotation [22]. The knee has several degrees of freedom to allow all these motions, see figure 1.2.

1.1.2 Stabilization

The passive stabilization mechanisms in the knee consist of four ligaments and a fibrocartilage meniscus, see figure 1.3. On both medial and lateral sides of the joint there are collateral ligaments which resist hyper adduction and hyper abduction motions; the lateral collateral ligament (LCL) and medial collateral ligament (MCL) respectively. Internally there are two cruciate ligaments; the anterior cruciate ligament (ACL) and posterior cruciate ligament (PCL). The ACL prevents the tibia from traveling too far anteriorly on the femur and hyperextension of the knee while the PCL prevents the tibia traveling too far posteriorly on the femur and hyperflexion of the knee [22]. The ACL runs between the posterior of the femur to the anterior of the tibia while the PCL runs anterioinferior of the femur to the posterior of the tibia. This creates an X in the intercondylar notch (as described later) on the distal end of the femur, which is where it gets its name of cruciate. Finally, there are two C-shaped meniscus disks, one medial and one lateral. This meniscus is a soft tissue which is secured to the tibial condyles and continuously conforms on the femoral condyles to create a stable surface during flexion and extension of the knee.

The active stabilization comes from the musculature which crosses over the knee. These muscles primarily provide the motion, however they also help stabilize when contracted during motion. These muscles consist of the quadriceps group, ham-
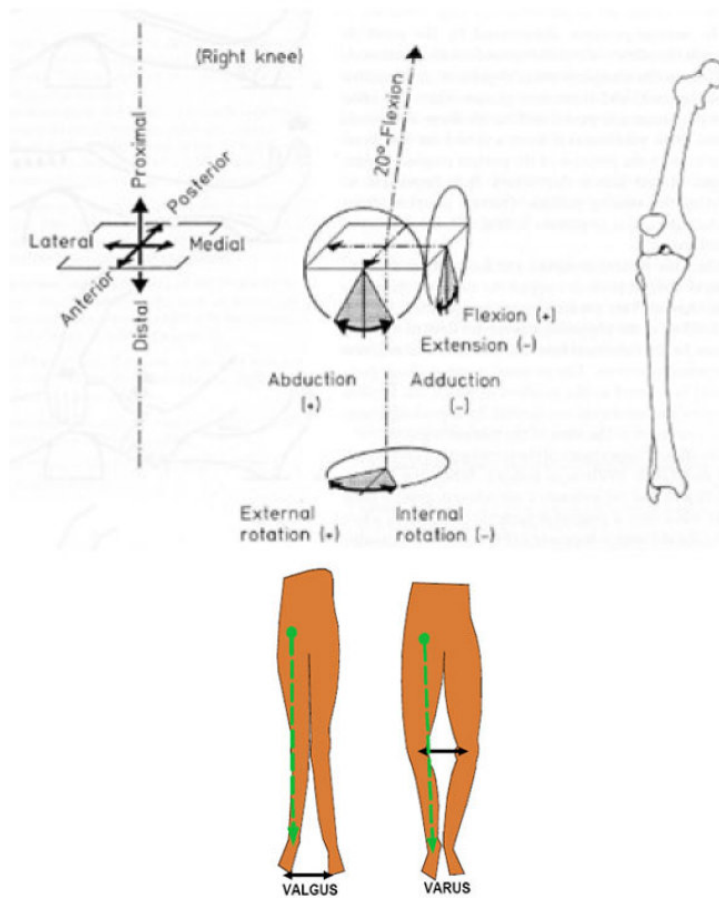
Figure 1.2: Degree of Freedoms of the Knee Joint

string group and triceps surae. The quaricpes (i.e. rectus femoris, vastus lateralis, vastus medialis, and vastus intermedius) all converge onto the quadriceps tendon which encapsulates the patella and continues as the patellar tendon inserting at the tibial tuberosity, see figure 1.4 and 1.5 [52]. The force from the quadriceps pull the tibia anteriorly, causing an anterior shear force on the knee joint as well as the extension motion. The hamstring balances this anterior pull from the quadriceps
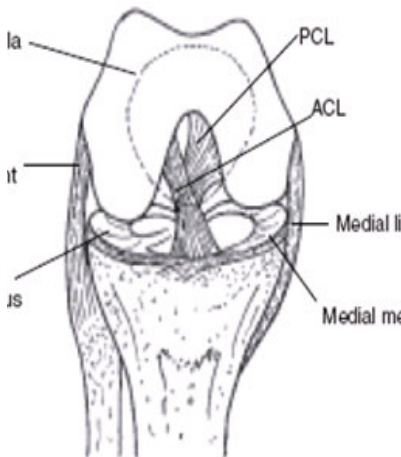
Figure 1.3: Ligaments in the Knee Joint [21]

and contributes the flexion motion. The hamstring group inserts posterior on the tibia and fibula, and consists of biceps femoris long and short head, semimembranosis, and semitendonosis. All but the biceps femoris short head originate on the pelvic bone at the Ischial tuberosity while the short head originates on the femur. The last muscle which aids in stabilization is the gastrocnemius, which is along the tibia, attaching to the femur.

1.2   The ACL

Injury to the ACL is a common knee injury which drastically hinders the knee joint stability, and in turn the person's stability while on their feet. ACL injuries begin at lower strains when fibres in the ligament start to break down. From this point on, further injury is incurred with further strain until complete rupture. This strain results from the tibia translating too far anteriorly of the femur, see figure 1.6. Most ACL injuries happen during sporting events, when the participant is fatigued [7]. It has been shown that the majority of the motions which put the ACL at a high-risk of injury include sudden deceleration, directional change and landing [54, 4]. Basketball, soccer, handball, netball and volleyball have high incidences of ACL injuries due to the increased frequency of these high-risk motions [21].

4
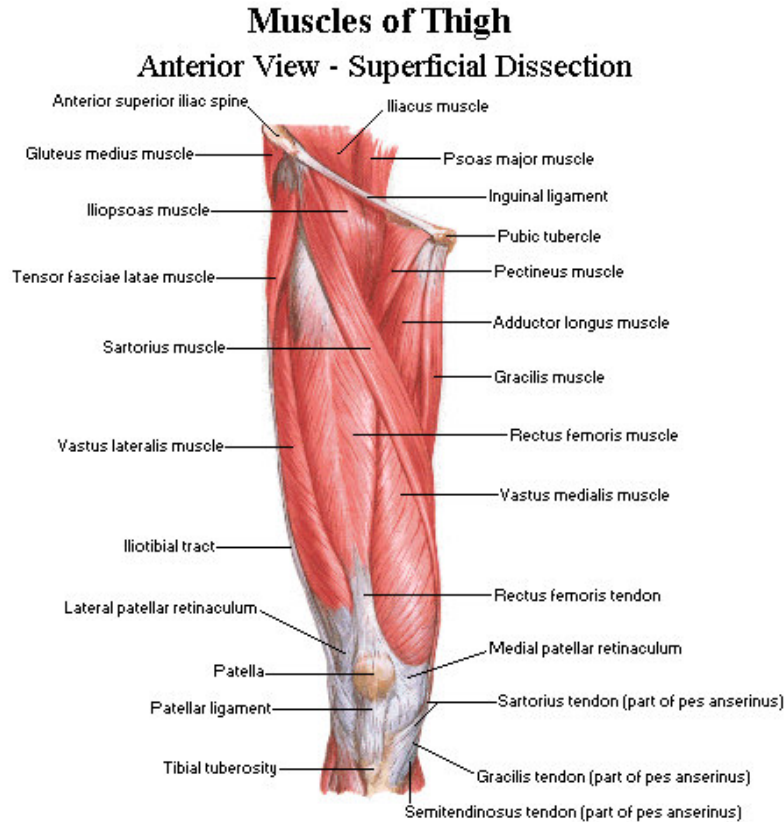
Figure 1.4: Anterior View of the Muscles in around the Femur [1]

1.2.1 Prevalence of ACL Injuries

The ACL is the weakest of the 4 stabilizing ligaments in the knee [22], which is likely the reason, in part, that it tears so often. Thousands of people injure their ACL every year in the US where 50 000 to 100 000 of those injuries are full ACL ruptures which require surgical reconstruction [36, 37, 45, 19]. Fifty percent of these injuries occur in the age group of 15-25 years old [19, 47]. This has become the 6th most common orthopedic surgery in the US, every year costing $2 billion in surgical costs alone [21].

Seventy to Ninety percent of all ACL injuries occur under non-contact scenarios, where nothing in contact with the knee during the injury [21, 43, 4, 47]. Also, the injuries occur during the landing phase as opposed to the take off phase of the motion [10]. These injuries therefore come from different landing techniques and maneuvers. However, it is currently unknown exactly type of motions causes the injury, or when the injury occurs during this motion.
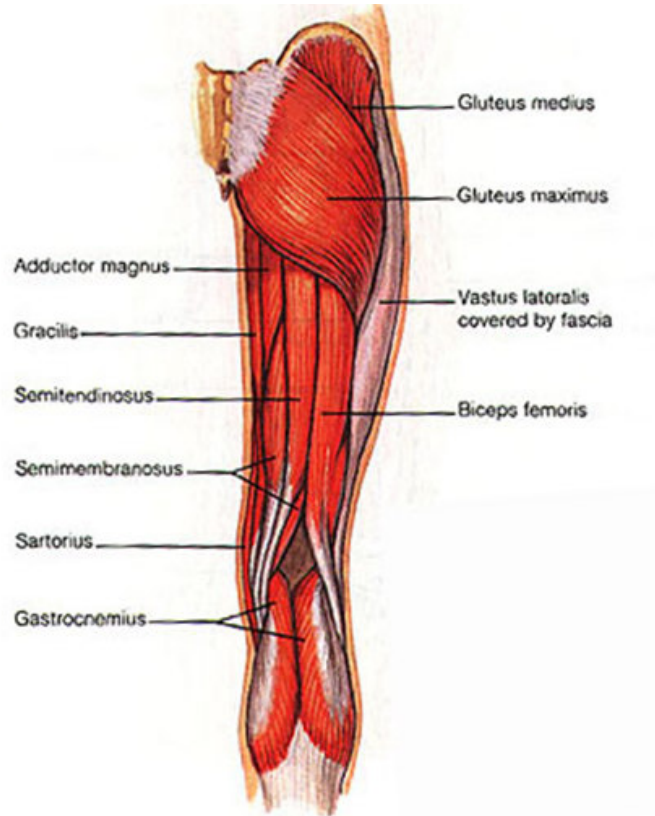
Figure 1.5: Posterior View of Lower Extremity Muscles [2]

1.2.2 Gender Difference

Females are 4-8 times more likely to injure their ACL compared to males [21, 28, 10]. As the female participant numbers in sports have been increasing the trend of female ACL injuries has become very apparent. A survey of ACL injuries in NCAA soccer and basketball over a five year period was done in 1995. The difference between male and female ACL injury incidences were significant when expressed as an injury rate, reported per 1000 athlete-exposures where 1 athlete-exposure is described as either 1 practice or game, and as a percentage of all injuries reported. In soccer players, females had an injury rate of 0.31 compared to males at 0.13. In basketball, females had an injury rate of 0.29 compared to males at 0.07. These studies show that females have significant increased risk during athletic activities [4].

1.2.3 Complications due to ACL Injury

It is very important to investigate these injuries as it has been shown that knees with ACL injury are likely to experience long-term problems, and with the majority of injuries occurring in athletes of such a young age this is a cause of great concern. Eighty percent of athletes cannot return to the same level of activity after
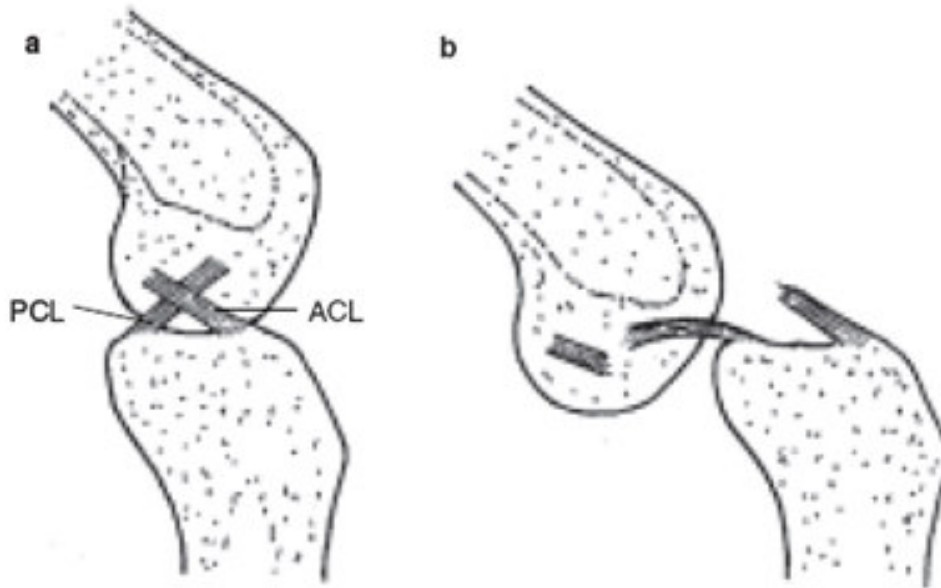
Figure 1.6: Translations of femur and tibia during ACL tear [21]

an ACL reconstruction surgery [39]. Some complications have been shown to include meniscal lesions, minimal knee function, and increased risk and occurrence of osteoarthritis(OA) [36, 45, 29, 27]. In a study of 223 injured ACL patients, 70% of patients had arthrofibrosis of the joint and 30% had other complications such as Cyclops syndrome and osteoarthritis [33]. The increased risk and development of OA is likely the effect of additional anterior tibial translation due to a weakened ACL stabilization as well as the change in contact forces in the knee as the kinematics change when the ACL is no longer influencing the motion. Reconstructed ACL's have a slightly smaller risk of OA onset because the ligament is replaced, however compared to non-injured ACL knees any ACL injury has significantly greater chances of OA. In one study, by year 20 after the ACL injury 100% of the knees had OA [29]. In another 12 year study, 51% of ACL injured knees had OA and 75% of knees were considered symptomatic [28].

1.3   Mechanism of ACL Injury

Since the majority of ACL injuries are incurred during a non-contact situation, it is thought there may be several different internal and external mechanisms which influence the injury; kinematic influences, neuromuscular patterns, ground reaction forces, and anatomical configuration in the joint. There have been many studies

surrounding all these influences as to whether they induce additional strain on the ACL, in turn causing injury or not. The following will explore the current theories as to why the ACL is injured. With the increased vulnerability of females to the injury, most studies that address at-risk ACL's looks at the differences between genders.

1.3.1 Kinematic Influences

There are several degrees of freedom to consider in the lower limb; the hip, ankle and knee. Each experience different moments and flexion angles throughout active motion. During landing, several kinematic and kinetic observations have been made at the peak ground reaction force such as peak knee valgus moments, peak knee extension moments, and increased anterior tibia shear force (ATSF). The ATSF is the most direct loading mechanism on the ACL, and it alone causes the greatest strain compared to knee valgus/varus moments and internal/external torques on the knee. However, when a knee valgus moment is applied along with ATSF it produces the greatest loading condition on the ACL [53, 31]. Other studies have shown that women tend to land with a valgus moment at the knee, compared to men who land with varus moments [10, 53]. This could be one reason why females have a higher risk of ACL injury.

Another kinematic aspect of landing is the knee flexion/extension moment created as well as the flexion angle of the knee at the time of ground contact. Females tend to land with knee flexion moments, requiring the quadriceps to increase their force production to compensate, which causes an increased anterior tibial shear force. It has been shown that the ground reaction force can be used to predict the knee flexion moments, which are then used to predict the ATSF. Finally, the ATSF can be used to calculate ACL strain experienced [55]. The ACL has been shown to acquire more strain with decreasing knee flexion angles, with the greatest load bearing situation at full extension [21]. Females land with decreased knee flexion compared to males [55, 11, 9]. Females have greater knee valgus moments, knee flexion moments, greater ground reaction forces and decreased knee flexion angles, all leading to the increased probability of ACL injury.

1.3.2 Neuromuscular Patterns

As mentioned above, one form of ACL loading comes from the anterior tibial shear force (ATSF). During landing, quadriceps are loaded eccentrically to help dampen the impact however this causes an (ATSF) [5, 54]. This shear force occurs from the quadriceps pulling through the patella tendon on the anterior portion of the tibia anteriorly compared to the distal end of the femur [21]. The maximum ATSF that can occur is found near full knee extension [5, 43, 54]. The hamstring is activated during landing which creates a posterior tibial shear force meant to oppose the ATSF consequently reducing the force through the ACL. It has been found

that women have lower absolute isometric, concentric and eccentric quadriceps and hamstring strengths compared to men and also have a much larger quadriceps to hamstring ratio, meaning the quadriceps is significantly stronger than the hamstring [5]. This increase in quadriceps to hamstring ratio could attribute to the increased female incidences of ACL tears as there is additional ASTF on the joint causing extra strain in the ACL. It has been shown that after 10 degrees of flexion, the hamstring contribution if equal to the quadriceps force, has a significant effect in decreasing the strain through the ACL [32].

Many studies have shown the relationship between the quadriceps and hamstring muscle groups and their influence on the ACL loading mechanisms, but few have considered the gastrocnemius as an antagonist to ACL strain. Fleming *et al* found that the gastrocnemius was indeed an antagonist to the ACL strain, especially near full knee extension. When the quadriceps contributions is coupled with the gastrocnemius the ACL strain increased further, when coupled with the hamstring the strain only slightly increased as compared to solely gastrocnemius contraction [17].

Electromyography (EMG) studies of the preparatory phase of ground contact has shown significant differences between genders in muscle activation patterns [18]. Women have larger muscle activation patterns before landing; however their hamstring activation is much lower than males after the moment of contact during landing [9]. Since muscle activation can be correlated with muscle strength, this shows a difference between the male and female muscle forces on the knee during landing.

1.3.3   Ground Reaction Forces

The posterior ground reaction force (PGRF) is a key component to predicting the knee flexion moment, which has been related to ACL strain [43]. The PGRF causes a knee flexion moment which the quadriceps compensate for by applying a knee extension moment. This added quadriceps force will cause an increased ATSF and therefore an increased ACL strain [54]. There are three correlations which suggest that the ground reaction force(GRF) can be used in ACL loading predictions; the peak knee extension moment and peak ground reach force are strongly correlated, the peak extension moment and ATSF can be correlated, and finally the ATSF and the induced ACL strain can be correlated [55]. Females have been shown to produce much higher PGRF during landing as well as overall impact forces [55, 10].

1.3.4   Anatomical Configuration

The intercondylar notch width, INW, between the femoral epicondyles is a main predictor of the size which the ACL can be. A small width reduces the size that the ACL can be, which decreases the mechanical properties and the strength allowing for the ACL to injure easier [21]. To normalize the data between genders the notch

width index, NWI, is used. NWI described the ratio of the INW to the width of the femoral epicondyles, see figure 1.7. Females tend to have smaller INW and NWI [21, 15]. The cross-sectional area of female ACL is 40%-50% smaller than males, showing a significant difference in size between genders [15].
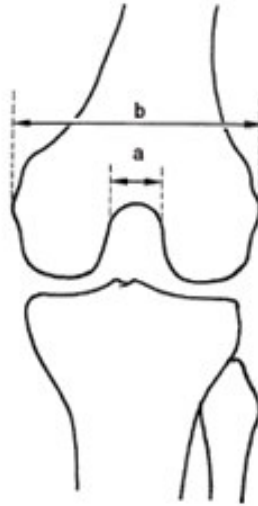
Figure 1.7: a - intercondylar notch width, b - width of femoral condyles [21]

1.4 Prevention Strategies

There are several suspected ACL injury mechanisms that cannot be changed or fixed to reduce the risk of ACL injuries. These include the size, material properties of the ACL itself and the notch width. However, other factors can be improved such as the kinematics of landings and the muscle activation (strength and timing).

In 1996, when the prevalence of ACL injuries had become a serious problem with athletes in all levels of sports, prevention programs started to be created. Several small scale prevention programs have been created and tested, most proving successful within localized groups of athletes, however the overall trend of ACL injuries has been unaffected. A 13 year study was completed using the National Collegiate Athletic Association Injury Surveillance System, which tracked the comparison between basketball and soccer as well as female and male ACL injuries, in both contact and non-contact situations [3]. Figure 1.8 shows the trend over the 13 years and there is no noticeable change in non-contact ACL injuries after 1996. Even though on a small scale these prevention programs seem to work, there is

currently no large scale solution that is effective at reducing the number of ACL injured athletes. Since there is still a need to discover the reason(s) for ACL injuries,
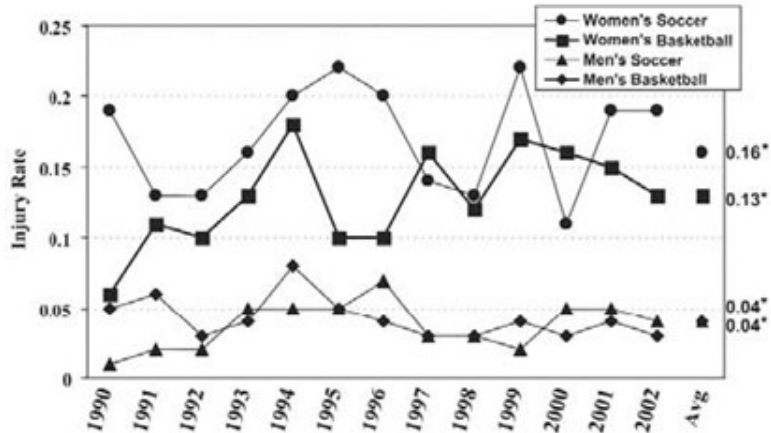
Figure 1.8: ACL injury rate over 13 year study [3]

more in depth research is required. This report discusses a new simulator which will give more realistic rationale for how and why ACL's are so readily injured.

Chapter 2

Current Research Methods

All the research up until now shows that ACL injuries are not very well understood, and so preventing this injury is very difficult. Investigating and researching the cause of ACL injuries is challenging due to the ethical restrictions on directly collecting strain from a real ACL or collecting reliable data on surrounding muscular influence during the injury. Measuring the actual force of the contributing muscles can only be accomplished with EMG and this is not an accurate method for capturing actual forces of specific muscles, only activation patterns. There are a handful of different methods for prediction on ACL injuries. The sections following describe the advantages and disadvantages of each method.

2.1   Kinematic Studies

Many different studies have been done comparing the kinematics and kinetics of landing and maneuver techniques during athletic motions, including comparisons such as male vs. female and injured ACL athletes vs. non-injured. These studies look at the knee, hip and ankle orientations and angular motions, segment velocities and accelerations and EMG readings from select muscles which cross the knee. The outcome of these studies show differences in joint angles at the instance of landing, segment velocities and accelerations, ground reaction forces and muscle activation profiles. This data can be used for predictions of higher risk motions and techniques. For instance, comparing women who had experienced ACL injuries to those without injury showed that injured knees have significant differences in neuromuscular activity and anterior-posterior shear force. The interesting finding was that there was no difference in peak hip and knee joint angles for both drop jumps and up-down jump tasks [39]. This is an interesting finding as it contradicts other studies which showed lesser knee flexion is more dangerous. This shows the difficulty involved in finding the cause of ACL injuries, since different studies find opposing results.

Common maneuvers used in these studies are single leg and two foot landing, plant and cutting and up-down jumping tasks [39, 38, 36, 11, 43]. From these results

researchers can infer risky motions and possible causes of ACL injuries However, the results are speculative since no actual ACL strain measurements can be made and in all these tests no ACL's were injured.

2.2 Video Analysis and ACL Injury

To capture an ACL tear, video footage can be analyzed. Recently Krosshaug *et al* took video footage from three different ACL injuries, one each from basketball, handball and skiing, and then reconstructed a three-dimensional kinematics model of the injury. This is the first method which captures the actual motion involved in an ACL injury. The photogrammetric model-based image-matching technique [25] creates 21 rigid segments in a hierarchical structure with the pelvis as the parent segment and overlays onto the athlete in the video, see figure 2.1. In the basketball study, Krosshaug *et al* used video footage from four cameras, each capturing the injury from different angles. From this skeleton model the joint angles, center of mass velocities and accelerations were calculated with Matlab [26].
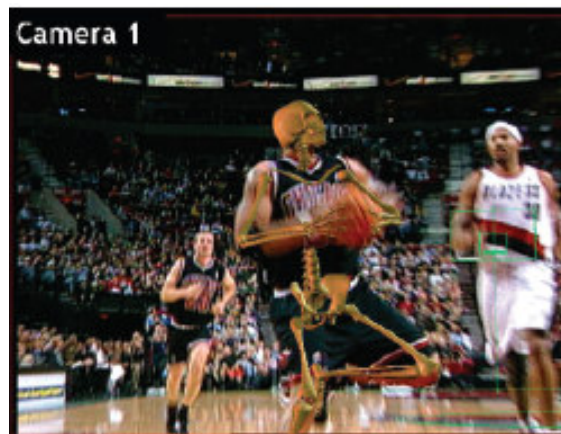
Figure 2.1: Skeleton overlay on basketball video [26]

This method is limited to capturing the injuries on video, with visibility of the athlete for the entire motion; the fewer cameras capturing the motion, the lower the quality of the results. Even though this method captures the actual injury, only the motion can be analyzed. Influences such as musculature are impossible to analyze, as this method is after the injury and the injury cannot be predicted ahead of time enabling EMG collection. Also this method takes an extremely long time, it is estimated to take 1-2 months to complete with an experienced operator.

This kinematic testing is great for tracking the motion during ACL injuries and high risk-motions. However, actual ACL strain cannot be measured. Modeling is an excellent way to overcome this and get actual ACL strain.

2.3 Modeling of Lower Extremity

The majority of modeling originates from kinematic testing data of human motion during different dynamic motions; generally the ones thought to be risky [40, 37]. The models are then used to calculate internal forces using inverse or forward dynamic techniques [12]. Muscles are usually added, however muscle addition is complicated because they cause an indeterminate system of equations, and the lines of action of muscles are not all straight as muscles wrap around bone and around other muscles and soft tissue.

The lower extremity is generally modeled as separate segments with defined joints given certain degrees of freedom to mimic ligament and bony influence. For instance, Pflum *et al* [40] used 10 segments for the lower extremity with a total of 23 degrees of freedom including a three degree of freedom ball and socket joint at the 3rd lumbar vertebra to model the upper body motion [40]. Models consisting of only the lower portion of the body must compensate for weight and inertia from the upper body motion. Usually the equivalent weight is added to the pelvis, as done by McLean [37] this is a good compensation, however it misses out on the influences of the arms and the inertia from the trunk.

McLean [37] took motion trial data and used a forward dynamic 3D model with wobbling masses attached to the skeleton with a linear translation spring and damper to solve for joint loading. Sixteen muscles were attached to the model, with moment arms assumed to be constant and based on published data. A three-element Hill Model was used for force generation of the muscles. The model was used for neuromuscular control on knee joint loading compared to the anterior drawer force, valgus moment and internal rotation moment.

These models work quite well to find internal forces and moments on the lower joints. Their limitation lies in the lack of information about muscle influence and soft tissue mechanical properties. Modeling works very well with the kinematic testing to achieve the most reliable motions and internal forces produced.

2.3.1 Anybody Software

Only a few modeling systems have made it to commercial market. The Anybody Project is one of only a few models which allows users to input motion profiles. Using inverse dynamics and carefully developed optimization algorithms, the Anybody model solves for individual muscle activation profiles throughout the motion. The Anybody model consists of over 200 muscles modeled as Hill-type muscles, with compensation for muscle wrapping [41]. The skeleton with lower extremity muscles showing can be seen in figure 2.2. This model outputs the motion at all joints (both the input marker data and remaining reference points), muscle activation profiles for all muscles, suspected EMG data and segment kinematics (including velocities and accelerations).
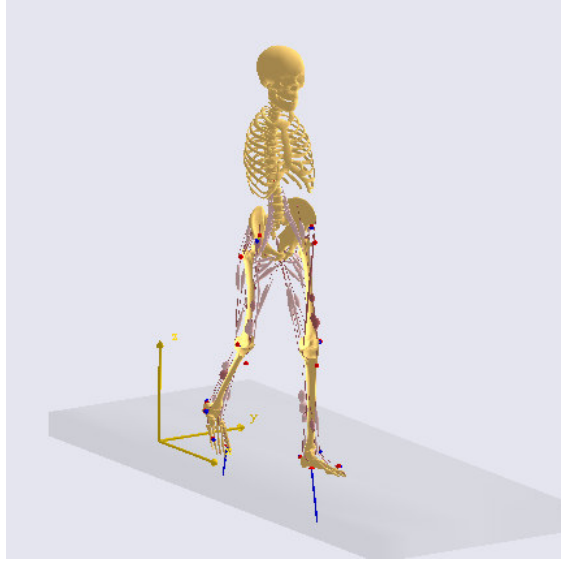
Figure 2.2: Anybody Skeleton with lower extremity muscles

This modeling system is very thorough at solving for muscle activations, body segment motions and joint moments. However it is not designed to look for injury in soft tissues such as ligaments. It uses joint motion restrictions instead of ligament attachment and influence.

2.4 Simulator

Even with all of these modeling and kinematic testing methods used to research the cause of ACL injuries, none of these methods actually measure the real strain in the ACL or the muscular forces. To study these influences, cadaver testing can be used.

Several knee simulators exist, all for different purposes and with different advantages and disadvantages; the majority of simulators are for knee prosthesis wear testing. Wear simulators concentrate on matching joint flexion angle and joint compressive loads for simple gait patterns [44, 14, 8, 13]. These simulators run high capacity dynamic cyclic testing on prosthesis, so they are designed for long run times at gait-like speeds and forces. One of the more advanced prosthesis simulators, the Purdue Mark II simulator, has accounted for high loads and rapid motions for athletic activities [30]. The femur and tibia are both attached to the ground through sleds at the ankle and hip which allows them to be flexed independently. This set up does not directly control the kinematics of the knee however the resultant influences from the external loads, geometry and soft tissues should provide

a more realistic 'natural' knee motion [30]. With this prosthesis simulator, faster motions are able to be tested for athletic people.

Prosthetic simulators are very helpful for wear testing, but they lack the physiological reactions the knee would experience and so do not have any real applications for injury prevention purposes. A new generation of knee simulators has come into existence to remedy this scenario. These simulators have started putting muscle contributions into the design as well as leaving all out of plane constraints free to move as they would with ligament and soft tissue influences.

The first attempt at a realistic simulator was created at McGill University by Szklar in 1987. A simple dynamic knee simulator was developed, where it subjects the knee to a prescribed time-history of the joint compressive loads and joint flexion angles. This was the first simulator to target physiological contributions to knee dynamics. Szklar's simulator fixed the femur to a dynamometer, and all the forces were transferred through the tibia. Two hydraulic actuators attached to flexible cables acted as the knee flexor and extensor, the extensor cable is attached to the patella so as to incorporate the patellofemoral joint in the motion. These actuators applied forces to follow the time-history of the knee, while all other conjunct and passive motions were left unconstrained. This design does not accurately accommodate for the ground reaction forces, as these forces have been incorporated into the flexor and extensor cable forces. This simulator is good for realizing the desired joint compression force and flexion angles; however this does not simulate proper anterior-posterior shear loads the musculature would normally provide [48].

The McLean simulator, see figure 2.3, is directly based off the Szklar simulator and designed for level and stair (ascending and descending) gait. McLean took the ground reaction forces components from the extensor/flexor cables in the Szklar simulator and separated them into their own cable contribution. The two components of the ground reaction force deemed influential are the axial load up the tibia and the moment caused by the moment arm of the tibia to the ground and the vertical ground reaction force. This solves the anterior-posterior shear load problem in the original Szklar simulator because now the flexor and extensor muscle contribution can resist the ground reaction forces instead of causing them. Still the muscle reactions are programmed to ensure flexion angle is maintained while the ground reaction loads are being applied [35].

A different design has come from Kiguchi *et al.* They developed a physiological knee motion simulator which is based on the length displacement patterns of the ACL and PCL over flexion angles of 0-90 degrees at the knee joint as opposed to the joint loading as was the case for the previous two simulator examples. The data used for the ACL length displacement patterns came from a study where a cadaver knee was manually flexed and extended with excursion wires implanted in the midsubstance of the anterior, medial and posterior ligament positions [42]. To simulate the muscular flexion-extension of the knee, four wires were pulled by DC motors. Two wires were attached at the patella and two to the posterior part of the proximal tibia. Fuzzy neural control was used to solve for the muscle reactions required to
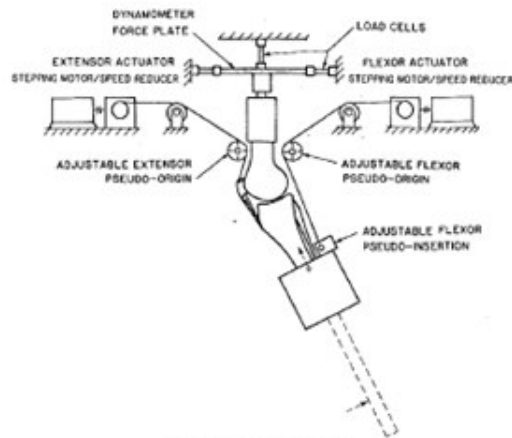
Fig. 1(a) Muscle actuation
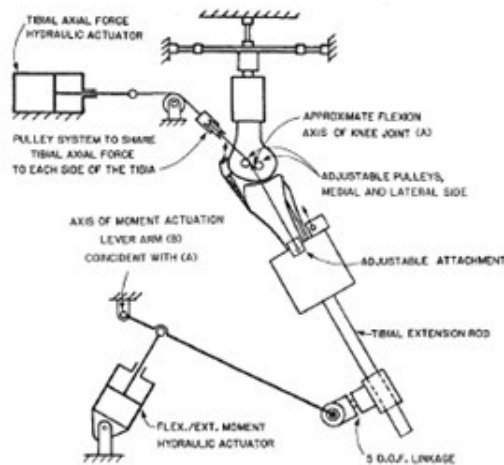
Fig. 1(b) Foot-to-floor reaction actuation. For clarity, the moment actuation lever arm axis B has been shown displaced. In the simulator, it is coincident with the approximate knee joint flexion axis A.

Figure 2.3: McLean Simulator Configuration [35]

achieve the required length displacement of the ACL and PCL. This simulator reproduced physiological knee motions well, however the length displacement of the ACL was limited because it was collected with manual flexing and extending, and had no muscle influence or ground reaction forces [23].

Most of these simulators only incorporate simple gait motions affecting the knee kinematics; however ACL injuries tend to occur with large decelerations, high loads and directional changes. This requires much faster actuators and motion of the joints.

The Hashemi *et al.* design of a simulator is the first to attempt motions faster than simple gait. Since ACL injuries occur during high speed motions, this generation of simulators will help to make huge advancements in understanding the

mechanism(s) involved in ACL injuries. This simulator incorporates two electric actuators, which are used to simulate the muscle actions, as well as a drop weight on an impact-plate set up, which is used for the ground reaction force on the tibia, see figure 2.4 [20]. It has been designed so that the muscle actuators have a set pretension just before the mass hits the impact-plate to mimic the preemptive nature of muscle, which anticipates landing, and then continues to hold that load for the entire motion. This simulator has incorporated the high speeds anticipated in high-risk motions for ACL injuries, however the muscle influence consists of holding a single tension which is not a physiological reaction the knee would experience.
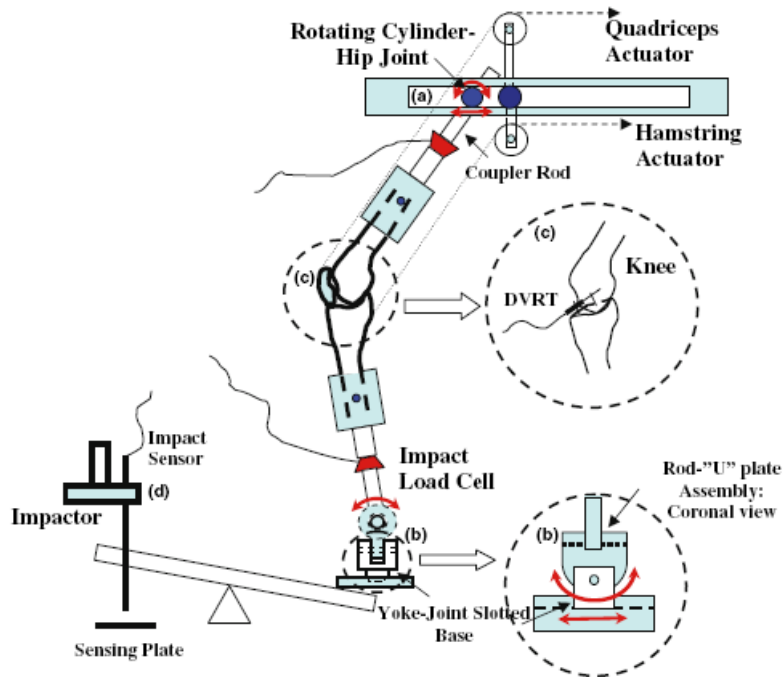
Figure 2.4: Hashimi et al Simulator Design [20]

Withrow *et al.* developed a simulator in which the valgus/varus and internal/external parameter could be set, see figure 2.5. A weight dropping on the proximal end of the femur rod applies the compressive force for the landing on the knee and there are three muscle groups incorporated; the quadriceps, hamstring and gastrocnemius. These muscles are represented by aircraft cable attached to the knee on one end and independent tensioning mechanisms, meant to hold a pretension on the muscle groups during the landing motion. This simulator is good for comparing different anatomical configurations as the hip and ankle can be moved to different positions before the weight is dropped. However, the position of the ankle and hip remain constant throughout the entire landing motion. This is not true to

the exact relationship between the joints during landing, as they can translate and rotate independently to accommodate the motion and stabilize the limb. Also the muscle contribution is simply a constant tension, not the true muscle activation profile [53].
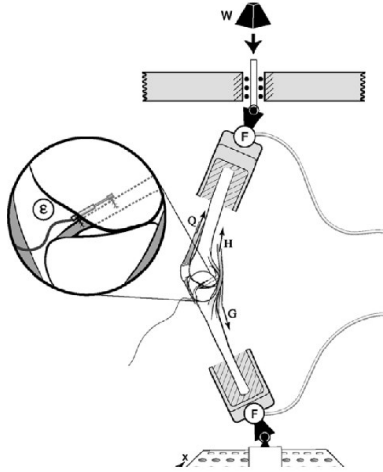
Figure 2.5: Withrow et al Simulator Design [53]

To date, there is no method for analyzing ACL injuries with all variables considered, specifically the neuromuscular, anatomical and kinematic motion. The simulators allow for actual ACL strain to be measured however they lack true muscle and ground reaction forces. Kinematic testing can analyze the muscle reactions through EMG, measure ground reaction forces and only calculate what they suspect the strain on the ACL will be. Finally, video surveillance is unique in that it captures the motion of an actual ACL tear, however no EMG or ground reaction forces can be taken.

2.5 Improvements for Present Simulator

These simulators of similar style lack the physiological muscle contribution. The inclusion of the muscle profiles will add a new level of realism in the simulator. The motion will be driven by the joint motion (hip and ankle) instead of the knee loading or joint angles, as in the Szklar *et al.* simulator [48]. This allows natural knee reactions to the hip and ankle motions. The Anybody software plays a large role in allowing the present simulator to have the muscle contribution, however the simulator is not limited to the use of this particular software and can be adapted in the future as deemed necessary. This initial design of the simulator will allow increasingly realistic knee kinematics to be performed in the future. This improves

upon most simulators to date which use only a pre-determined tension for the whole motion, eg. the Withrow *et al.* and Hashemi *et al.* simulators [53, 20].

Chapter 3

Design

The aim of this current simulator is to incorporate the realistic muscle reaction forces during different landing techniques and directly correlate those with the ground reaction force and leg motions. All aspects of ACL injury research will be incorporated. Kinematic testing will be done to collect motion profiles for three common, risky basketball maneuvers. With this motion data, Anybody software will be used to calculate the muscle profiles over the entire motion. Using the muscle profiles, this simulator will be able to apply muscle activation profiles to the joint during the different motions. A 6-axis controller is used to ensure all the actuators are moving in sequence based on of the Anybody Model timing. This simulator will apply simple gait and landing motions to a cadaver knee. While the simulator produces the motion, a labview program will collect load cell data for muscle forces and DVRT readings for the ACL strain.

3.1   Concept of Design

This thesis will concentrate on a 2-dimensional system, operating in the Y-Z (Sagittal) plane, incorporating flexion/extention of all lower extremity joints. The global coordinates used for this design are illustrated in figure 3.1. The design of the simulator must consider all parts of the process required for the simulation to ensure that all aspects of ACL injury, as outlined in the previous chapters, are covered. The following process flow is expected;

1. Designing mechanical hip and ankle

2. Motion capture of an activity

3. Collecting muscle force profiles and joint motion from Anybody Software

4. Creating a program to move joints and control muscle profiles compiled into groups
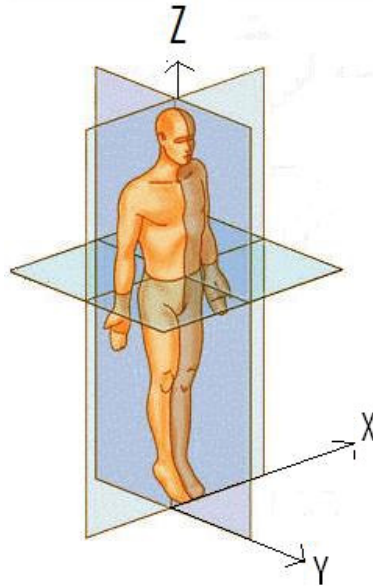
Figure 3.1: Orientation of the Body in the Simulator

5. Running simulation

6. Measuring ACL strain

7. Altering muscle forces and repeating simulation

From this several consideration have to be made in the design; the actuator selection, the frame design, the joint design, the controls of the system, and the data collection.

In figure 3.2 the overall concept can be seen.

3.2   Actuator and Motor Selection

Actuators were chosen that accommodated for the velocity and force of the joint motions at the hip and ankle as well as the muscle activation profiles. Two different types of actuators will to be used for the muscle and joint components, as their requirements are very different. Muscles have very little motion but must hold high loads, whereas the joints have a lot of motion by comparison while also applying the ground reaction force. These values, for the purpose of choosing appropriate
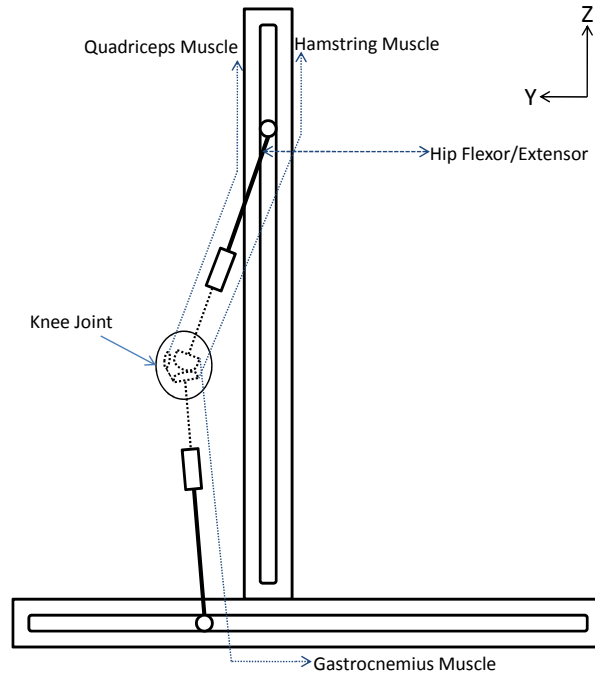
Figure 3.2: Concept of Design

actuators, were based on current research and kinematic testing. Due to limitations of connections in the lab, electromechanical actuators were the only style of actuators and motors sourced.

3.2.1 Muscle Actuator Selection

The goal of the muscle actuators is to be able to contribute the same dynamic forces to the knee joint as normal muscles would do. This means they should contract and hold the expected force which match what the muscles would realistically contribute throughout the entire motion. Including individually all the muscles that influence the lower limb would creates too complicated of a system as there are well over 30 muscles in the leg, so the muscles which influence the flexion/extension of the knee and hip are combined into 4 resultant muscle groups; the quadriceps, hamstring, hip flexor/extensor, and calf muscles. Table 3.1 shows the muscles which are included in each group.

To find the required force production of these muscle groups an assumption was made; the total force production of the group is assumed to be the sum of force

Table 3.1: Muscles included in each Muscle Group

Muscle Group	Included Muscles
Hip Flexor and Extensor	Iliacus and Psoas
	Pectineus
	Gluteus Maximus
	Gluteus Medius
	Gluteus Minimus
Quadriceps	Rectus Femoris
	Vastus Intermedius
	Vastus Lateralis
	Vastus Medialis
Hamstring	Biceps Femoris Long Head
	Biceps Femoris Short Head
	Semimembranosis
	Semitendonosis
Calf	Gastrocnemius Medial Head
	Gastrocnemius Lateral Head

produced by each muscle. Table 3.2 shows the forces used which is taken from McLean *et al* [37].

The maximum contraction distance and average time the motion takes are used to calculate the velocity with which the muscle contracts. The contraction length is assumed to be 30% of the overall length. For the muscle groups, the shortest contraction length of all the muscles in the group is used for the required contraction distance. The timing of a jump landing, in the worst case scenario, should last approximately 200ms [40]. The velocities used are tabulated in Table 3.3.

Table 3.2: Maximum Muscle Force

Muscle Group	Maximum Force
Hip Extensor	1300N
Hip Flexor	800N
Quadriceps	5180N
Hamstring	2480N
Calf	1605N

These values are used to compare different actuators to find the appropriate one for this application. Tolomatic actuators (Tolomatic Inc., Hamel, MN) were selected as they had the best fit for the motion requirements. For simplicity, the same RSA32 model actuator (see Appendix A) was chosen for all four muscle groups.

Table 3.3: Muscle Change in Length and Maximum Velocity Expected

Muscle Group	Max Contraction Distance	Contraction Velocity
Hip Extensor	0.043m	0.22 m/s
Hip Flexor	0.031m	0.15 m/s
Quadriceps	0.025m	0.126 m/s
Hamstring	0.033m	0.16m/s
Calf	0.015m	0.076m/s

3.2.2 Joint Actuator Selection

Because of the large distances that the joint components must travel, belt actuators are required. The setup will have the hip joint tracking the resultant Z motion, while the ankle joint tracks the resultant Y motion. This requires two belt actuators which can match the force and velocity of the landing from a jump. From different kinematic trials, the maximum displacement, velocities and force from different athletic motions were used as data for actuator selection [26, 34]. The actuators velocity and force were based on the X, Y, Z motions of the center of gravity of the person. The ground reaction force was used as the limit of the force of each axis. The force in the vertical direction will be assumed by the Z axis and the anterior/posterior direction will be assumed by the Y axis.

The results from the Krosshaug *et al.* kinematic reconstruction of the basketball injury describes the velocity of the center of mass and normalized ground reaction force in the vertical, anterior/posterior, and medial/lateral directions [26]. Also, McKinley *et al.* tracked the hip marker velocity and measured the vertical ground reaction force during then landing from a jump [34]. These values are summarized in Table 3.4 and Table 3.5.

Table 3.4: Maximum Velocity

Direction	Maximum Velocity
Medial/Lateral	3 m/s[26]
Anterior/Posterior	2.5 m/s[26]
Vertical(from two sources)	5m/s [26]
	2.8 m/s [34]

Table 3.5: Ground Reaction Forces

Direction	Force at Ground Contact	Maximum Ground Force
Medial/Lateral	0N	1250.78N[26]
Anterior/Posterior	833.85N	1667.7N [26]
Vertical (from two sources)	1667.7N	3335.4N [26]
		3959 N [34]

To help simplify the motion required for the lower extremity, the resultant Y and Z displacements are used on the ankle and hip respectively. This allows the design

to have two stationary Macron belt actuators(Macron Dynamics Inc., Croydon, PA). 14H Macron belt actuators (see Appendix B) were chosen for the required motion profiles.

3.2.3 Motors and Drivers

Danaher Motion brushless motors(Danaher Motion, Radford, VA) were chosen for their performance and reliability. The Tolomatic actuators are paired with the AKM42J motors and the Macron actuator are paired with the AKM73P motors, see Appendix C for motor specifications.

Also from Danaher Motion, two different AC servo drivers were chosen. The S200 driver was chosen to mate with the AKM42J motor, and the S600 driver to mate with the AKM73P motor. This pairing is from Danaher Motion, for the best matched driver to the chosen motors.

3.2.4 Power

The AKM42J motors require a single phase 240V power supply and the AKM73P actuators require a 3-phase 240V power supply. Additionally, a 24V DC power supply is needed for auxiliary functions in the actuator drivers as well as supply power for the controller.

3.3 Simulator Design

The aim and challenge of the design for the simulator is to construct a system that holds a cadaver knee specimen while being capable of initiating the motion of the lower extremity. To ensure that the knee kinematics stay true to natural motion, the knee specimen must have all the soft tissue, muscle and skin removed leaving only the four knee ligaments (LCL, MCL, ACL, and PCL), the patella and patellar tendon, and the meniscus. The knee must have femoral and tibial length past the condyles to attach to the simulator. The fibula must be cut just distal of the MCL and secured to the tibia.

The muscle actuators attach with steel cables to the average insertion point on the bone and to the origin point on the frame. These actuators are programmed to run in force control mode to ensure the contractile force of the muscles stays true to the estimated muscle force profile.

3.3.1 Frame

The frame is designed to ensure that six actuators are securely fixed to the same ground, while leaving room for future expansion. The Z axis actuator is to be

secured upright and the Y axis is to be secured on the ground. The actuators are mounted on the frame in a manner that mimics this; three of the muscle actuators are mounted above the hip connections and the 4th is mounted below the ankle. This requires the frame to have support above where the knee is mounted in order to secure three muscle actuators as well as the upright Z axis actuator. See figure 3.3 for the general outer frame structure.
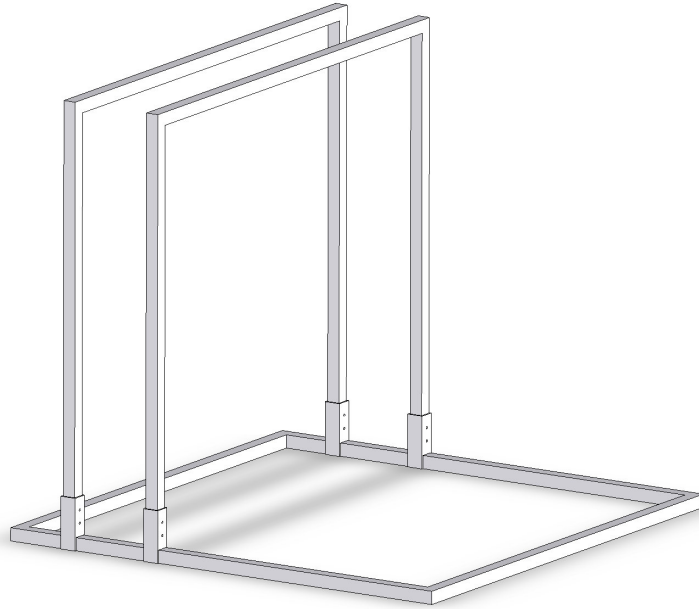
Figure 3.3: Layout of Frame

3.3.2 Joints

The lower extremity consists of 3 joints; the hip, knee and ankle. The knee joint is the cadaver knee specimen itself and the hip and ankle joints will be designed to mimic the natural hip and ankle motion. The simulator design will rigidly fix to the sled of the belt actuators, the ankle and hip joints with extensions which the femur and tibia will mount into.

Hip

The natural hip joint is a strong and stable ball and socket joint. There are many ligaments and surrounding muscles which keep the head of the femur (ball) in the acetabular cup (socket) leaving it with three degrees of freemdom (DOF); flexion/extension, abduction/adduction, and internal/external rotation. See figure 3.4 for hip joint diagram. To simulate this freedom, a ball and socket joint was created for the simulated hip. Below is the design for the hip and it's DOF, see figure 3.5. A ball bearing was used with a hole through the center for a rod end in which the femur extension attaches to. Then a socket is machined out of a block of steel which is used to attach to the actuator. The hip needs a range of $0°$ to $84.57°$ of flexion, according to drop-jump landing kinematic data [11]. This range of motion is produced from the rod end while the abduction/adduction and internal/external rotation are produced by the ball and socket rotation.
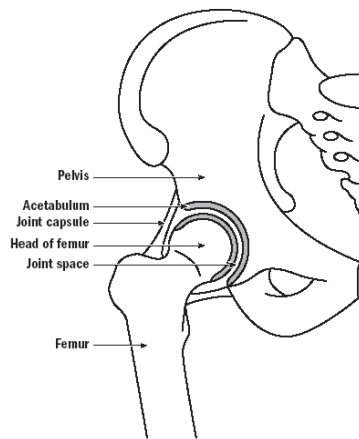
Figure 3.4: Hip Joint

Ankle

The ankle joint is a hinge type synovial joint, between the tibia, fibular and the talus, see figure 3.6. The same ball and socket joint design that was used for the hip joint was used for the ankle with additional restraint in the medial/lateral direction. This will restrict the abduction/adduction at the ankle like the hinge type joint does naturally. The ankle joint is rigidly fixed to a 3D load cell before attaching to the Y motion actuator. (refer to Section 3.6)

Both joints are equipped with simulated ligaments in order to limit their coronal plane motion and internal/external rotation, in the same manor ligaments act. A polymer tape is used, as it has minor stretch properties to allow for some out of plane motion but within realistic human joint capabilities. Also, these ligaments
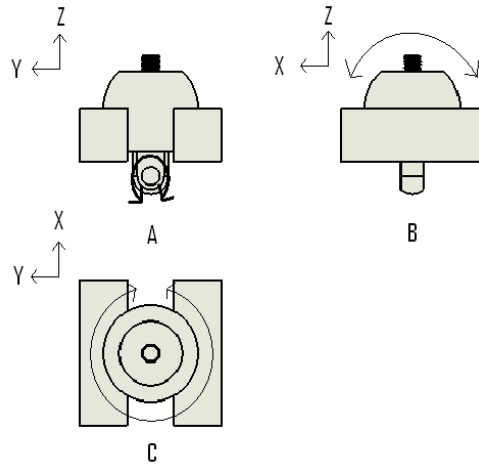
Figure 3.5: Degrees of Freedom of Hip Joint
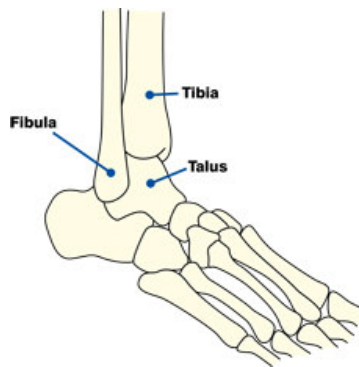
Figure 3.6: Ankle Joint

will attach from the turnbuckle/rod end connection to some ground such as the pelvis and foot, just as ligaments naturally do in the human leg.

3.3.3 Femur and Tibia Extension

To accommodate for the variability in the difference in the lengths of the femur and tibia, a turnbuckle, see figure 3.7, is used as the majority of the femoral and tibial extension length. This allows for the length to be fully adjustable, even with it all set up in-situ. Shultz *et al.* compared left and right lower extremities on healthy participants. They compared total length(femur and tibia), pelvic angle, quadriceps angles, etc [46]. They discovered that there is a significant difference between

29

left and right, so the simulator requires a method for adjusting the dimensions depending on the knee being used.

A cup is welded onto the distal end of the femur turnbuckle and the proximal end of the tibia turnbuckle. The cup is used to mount the femur and tibia, using eight screws to rigidly restrict any motion between the bone and turnbuckle. To avoid a bending moment stress on the bone, the cup is designed to envelop the entire bone, leaving only the femoral and tibial condyles visible. This results in approximately 5" of femur and tibia past the condyles. The turnbuckle on the opposite end of the cup is mounted to the hip and ankle ball and socket joints. Refer back to figure 3.5.
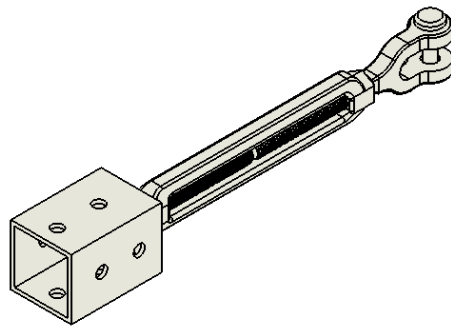
Figure 3.7: Turnbuckle used for the femur and tibia mounting

3.4   Muscle Attachment

The muscles are connected from the actuator down to the insertion point on the bone through either a pull/pull or push/pull cable, from Cable Craft (Cable Craft, Indiana, USA). The sleeves of the cables have two anchor points, one at the origin on the muscle group and the other end at the actuator. Then the cable is attached at the actuator and the other end at the insertion point on the bone. The hamstring attachment consists of a single cable through the tibial condyles (medial to lateral), the quadriceps attachment has 3 cable wraps through the patella, and the calf attachment consists of a metal strip wrapped around the femur. Finally, the hip attachment is rigidly fixed to the proximal end of the femur turnbuckle. There is a load-cell in between the cable and actuator to measure the force output of the actuator. A pull-pull cable is used for the quadriceps, hamstring and calf muscle groups as muscles can only function under tension. The hip flexor/extensor uses a push-pull cable as the hip flexor/extensor is designed to recreate the moment at the hip as opposed to the actual muscle contribution.

Because there is a $90^{circ}irc$ bend in the cable from the actuator to the mounting point on the hip and ankle friction is produced. The efficiency of the cables is not 100%, some force is lost to the friction. An efficiency calculation is required when calculating what the load cells are reading versus what force the cables are pulling at the knee. At 90, there is an efficiency factor of 1.09, see figure 3.8.
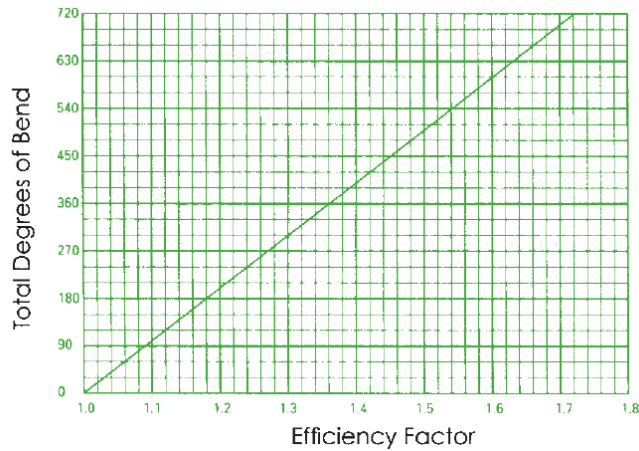
Figure 3.8: Muscle Cable Efficiency Graph

3.5　Final Design

Integrating all these design requirements, a final design is created, see figure 3.9 and figure 3.10. This design should allow for all high-risk motions which occur in the sagittal plane to be considered, with room for future expansion to include all out of plane motions. The simulator has 6 axis, refer to table 3.6 for description of which actuator represents which axis.

Table 3.6: Description of Axis on Simulator

Hip Flexor/Extensor	Axis A
Hamstring	Axis B
Quadriceps	Axis C
Calf	Axis D
Z Joint Motion (Hip)	Axis E
Y Joint Motion (Ankle)	Axis F
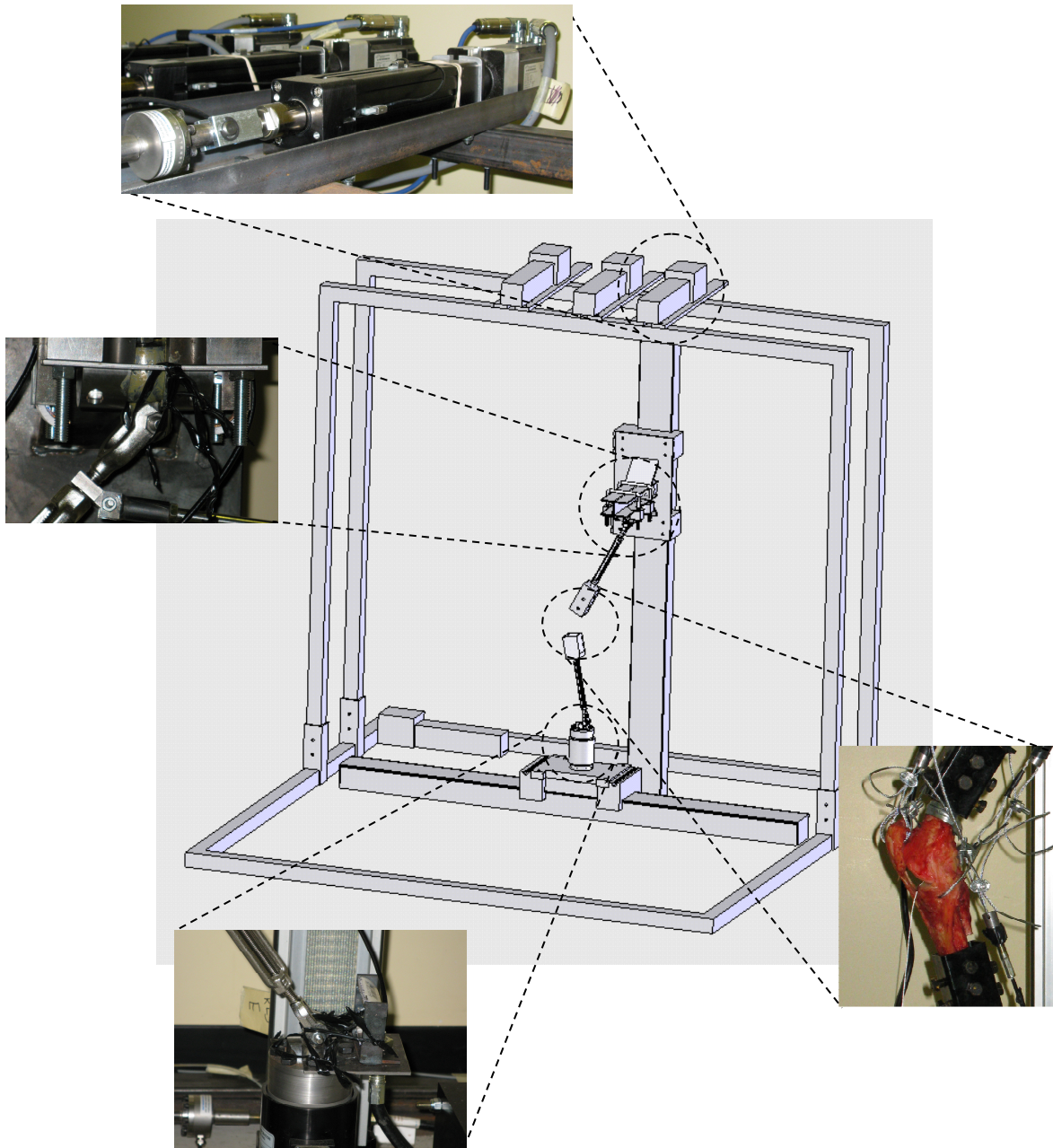
Figure 3.9: Components of Design
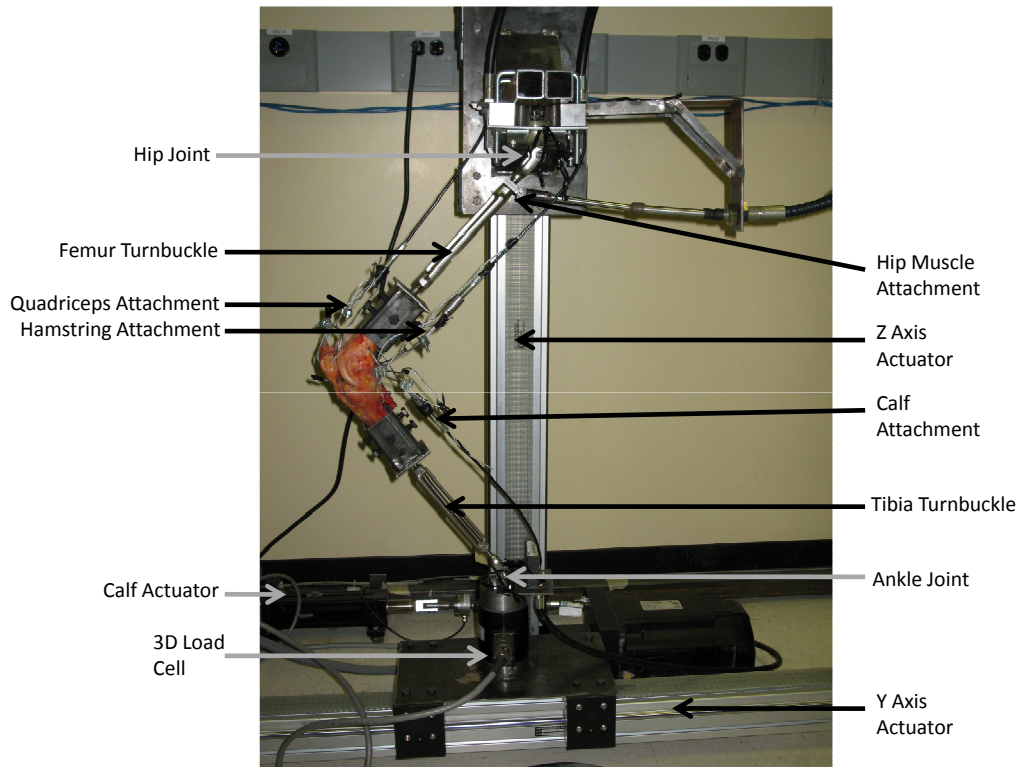
Figure 3.10: Final Design

3.6   Data Collection

Two different styles of load cells are used for data collection. The first style is a 1D load cell intended for the muscle actuators since they only pull in one direction. Omega Engineering (Omega Engineering, Connecticut, USA)load cells are used. The load cells are rated for $2000lb_f$ tension and compression. Each load cell has a different rating for V/lb_f (volts per pound force) they are as follows, see table 3.7.

Table 3.7: Load Cell Rating

Load Cell	V/lb_f
Axis A	0.010028
Axis B	0.010024
Axis C	0.010021
Axis D	0.010025

The second style is a 3D load cell, from Bertec INC (Bertec Corp, MI, USA), which measures force and moments in the X,Y, and Z axis. This load cell is used for capturing the ground reaction force at the ankle joint during the motion. The load cell has 6 channels measuring F_x, F_y, F_z, M_x, M_y, M_z.

To measure the strain in the ACL, a Differential Variable Reluctance Transducer (DVRT) (Microstrain, VT, USA) is placed on the ligament and will read the ACL strain through the entire motion, see figure 3.11.
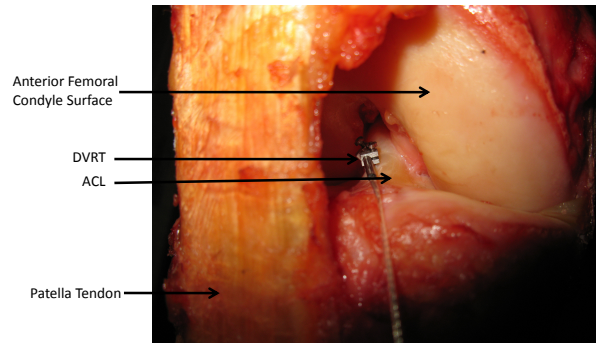
Figure 3.11: Mounting of DVRT on the Anterior side of the ACL

All data collection will be done through Labview (NI Labview, Austin TX, USA). A program collects the load cell and strain gauge data in time with the motion. The program reads four 1D load cells, all six channels of the 3D load cell and the DVRT and attaches a time stamp for comparison. This makes it capable

of matching the expected muscle force profile by controlling the actual muscle force profile that the actuators are producing. Galil Motion Control (refer to Section 4.2 has a labview VI which allows the labview program to directly take readings from the Galil instead of having to construct a separate data collection system.

3.7   Specimen Preparation

The cadaver knee requires dissection and muscle cable insertion before it can be mounted into the simulator. The skin, muscle and tendons must be removed from the knee, excluding the patellar tendon. The 4 knee ligaments; ACL, PCL, MCL, and LCL should remain entirely untouched and undamaged. To ensure the LCL is supporting the knee properly, the fibula must remain stable(the distal mounting point of the LCL is on the fibula, not the tibia). To accomplish this, a screw is mounted through both the fibula and tibia,the fibula/tibia ligament remains intact, see figure 3.12.
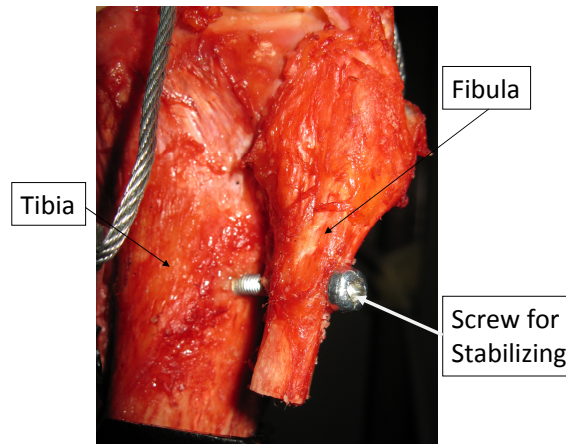
Figure 3.12: Screw through Fibula and Tibia for stabilization for LCL

The quadriceps tendon can be cut above the patella ensuring the entire patella is still encapsulated by the tendon, however excess tendon above can cause interference during motion, so an effort must be made to leave a minimal amount of this above the patella. All muscles and other tendons should be removed from the bone, along with all the fascia. The excess meniscus which protrudes from joint should be trimmed back but the meniscus inside the knee must be retained to ensure the kinematics of the knee remain true.

The muscle insertion points for the quadriceps, hamstring, and calf require a pre-drilled hole and steel cable to be attached. The quadriceps mounting location consists of three holes in the patella which the cable feeds through. Three holes instead of one are used in order to spread the large quadriceps force over more area on the patella. The hamstring cable mounts medially/laterally through the tibial condyles, posterior of the fibula however anterior of the MCL. Finally the calf mounts with a metal strip wrapped around the femur and the cable attaches to the posterior part of the bracket, see figure 3.13. See figure 3.14 for the location of all cable mounting locations. The final muscle attachment is the Hip Flexor/Extensor. This muscle is not attached to the knee, but the hip joint. The push/pull cable is rigidly fixed to the proximal end of the femur, just before the hip joint.
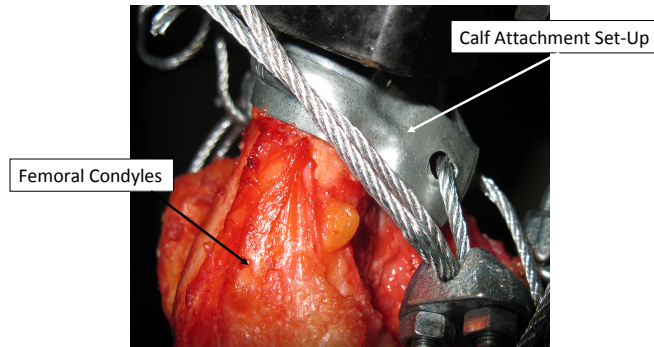
Figure 3.13: Posterior view of Calf Muscle Attachment Setup

Due to the biohazard of the human tissue of the specimen, the knee should be cleaned as much as possible. The nature of the simulator allows it to produce projectiles of unremoved tissue.
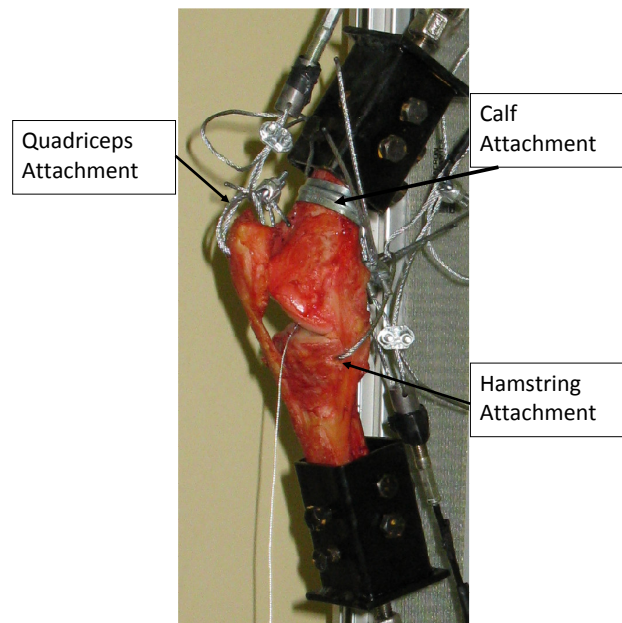
Figure 3.14: Attachment of Muscle Groups

Chapter 4

Simulator Operation & Control

The control of the simulator needs the ability to accommodate all ranges of high-risk motions. Basketball is one of the sports with the most incidences of ACL injuries, especially in the female athletes. Due to this, the simulator will aim at recreating basketball high-risk motions to analyze the influence on the ACL.

4.1 Kinematic Trial Data

To collect motion data for the high-risk maneuvers in basketball, two average athletes; one male(age 22, height 6'4") and one female(age 25, height 5'10"), completed kinematic trials. The trials tracked the motion through three different basketball maneuvers; the plant and cut, the single leg landing after a lay-up and the outstretched single leg landing during a running catch. Surface EMG was placed on the gastrocnemius and hamstring muscles for future validation purposes of the Anybody Software output. Fifteen markers were placed over the right leg of each participant at strategic bony landmarks, as well a 3D force plate was used to capture the landing ground reaction force during each action.

The participants were asked to perform each motion, ensuring they landed on the 3D force plate, in sequence. Five good trials of each motion was collected, good trials meant they landed on the force plate, all markers were still attached to the skin after the motion was completed, and the EMG produced appropriate readings. Stationary maximum voluntary contraction (MVC) weas performed before trials, which was used for standardizing the EMG readings. Figure 4.1 shows the set up of the male participant during the motion capturing.

This data will be used in the future for the high-risk motion simulation, however for the purpose of this thesis and validation of the simulator a simple gait model will be used. Gait data published Vaughan *et al.* is used for the validation of the simulator motion [49].
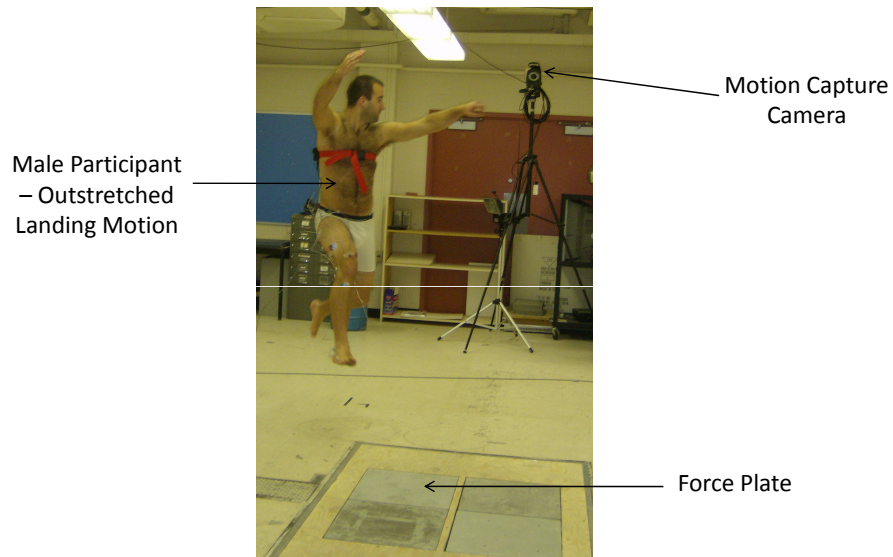
Figure 4.1: Motion Capturing Set-Up - Male Participant

4.1.1   Anybody Model

In the Anybody Software, there are two current published models for gait; gait-Vaughan and gaitUniMiami. For this thesis the gaitVaughan model is used, with a gait cycle of 1.3 seconds. This model uses the motion data and ground reaction force measurements from Vaughan *et al.*: Dynamics of Human Gait [49]. Markers on the skeleton model in the Anybody Software drive the motion of the lower extremity, see table 4.1 [16].

Fifteen markers from the Vaughan published data are inputted into the Anybody Model and the model is run [16]. From this the muscle force profiles, muscle EMG readings and joint motion profiles are calculated and used for the control and validation of the simulator. This data is outputted in 10ms time increments.

4.1.2   Adapting Muscle Force Profiles

The Anybody software outputs the individual muscle force profile, however the simulator operates with the muscles grouped. To group the muscle force profiles,

Table 4.1: gaitVaughan Marker positions

Marker Name	Marker Location
Right Metatarsal Head	right foot
Right Heel	right foot
Right Lateral Malleolus	right shank
Right Tibial Tubercle	right shank
Right Femoral Epicondyle	right thigh
Right Greater Trochanter	right thigh
Right Anterior Superior Iliac Spine	pelvis
Left Metatarsal Head	left foot
Left Heel	left foot
Left Lateral Malleolus	left shank
Left Tibial Tubercle	left shank
Left Femoral Epicondyle	left thigh
Left Greater Trochanter	left thigh
Left Anterior Superior Iliac Spine	pelvis
Sacrum	pelvis

the resultant force of all muscles involved is needed. From White *et al.* the origin and insertion coordinates for all muscles in the lower extremity were measured and published (See Appendix D [51]). The muscle insertion and origins are only given in terms of local coordinates different bony landmarks. Horsman *et al.* took a cadaver leg and measured the global coordinates of bony landmarks, which are used to relate the White *et al.* muscle insertion and origins to a global coordinate system [24]. The X, Y and Z angles were calculated from these coordiantes for the line of action of the muscles. With this each muscle from the Anybody Model output was broken into F_x, F_y, and F_z components and then each muscle groups is summed, $\sum F_x$, $\sum F_y$, and $\sum F_z$. From this the final resultant force is found with $F = \sqrt[2]{F_x^2 + F_y^2 + F_z^2}$. The location of the resultant muscle origin and insertion on the simulator is influenced by the ability to securely mount the cables into the cadaver knee. Using exact averages of the muscle origins for each group could not be used due to this limitation.

4.2 Control

With a system that has 6-axes in simultaneous control, the simplest control system was required to reduce the complexity of the simulator. The Galil (Galil Motion Control, California, USA) MC4060 6-axis controller was chosen due to it's extreme simplicity in programming motion and it's capability for data collection, see figure 4.2. Another convincing reason was it's capability to run some axes on force control while others on position control within the same program. The program will run through several array steps, having a time step of 10ms. The 10ms time step is

dictated from the format of the Anybody software output which is given in 10ms time steps.

Figure 4.2: Galil 4060 Controller

4.2.1 Force Control Mode

The force control mode on the Galil operates by comparing the analog input channel and the programmed array point. The controller adjusts the signal sent to the motor until the two inputs match. This is a continuous and quick process, where the first axis reads analog channel 1, etc. This allows the muscle force profiles to ensure that for the entire 10ms step the actuators hold the appropriate force and do not relax or transmit too much force. The design has the load cell inline with the muscle cables and wired into it's corresponding analog channel on the Galil, i.e. Axis A (Hip Flexor/Extensor) load cell is wired to analog channel 1. This allows the Galil to continuously correct the force which the actuator is outputting to match the value in the array, see figure 4.3.

The array and load cell analog input need to be the same units so the Galil can properly compare. The Galil in force control mode is configured so the analog input converts the voltage of the load cell to ADC counts where, $2048ADC = 10V$. For programming the muscle profile in ADC counts, the force required needs to be converted to the equivalent voltage of the load cell then to the ADC counts equivalent to that voltage.

4.2.2 Position Control Mode

The Y and Z axis motions are programmed in position control mode. Initially absolute positions every 10ms was used as this is the simplest method. However if the actuator reaches the point before the 10ms it stops moving and wait for the next time step. This causes the motion to become jerky and unrealistic to true
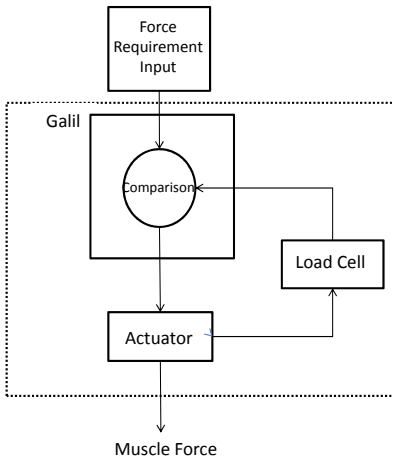
Figure 4.3: Closed look system

human gait. Programming it to reach the desired position exactly at the 10ms is extremely difficult.

It was found that running in velocity commands resolves the jerky motion. The velocity required to move the distance for each time step is calculated as the distance required divided by 10ms. The actuator travels at that speed for each 10ms, assuming the distance it has traveled is the distance required.

4.3 Galil Code

The program designed for the gait motion, and any future motions, is a simple array tracking program. Four arrays are created with the force values in ADC counts and two arrays with the velocities for the joints. At each time step the actuator will follow the respective corresponding array value, see Table 4.2 for array names and corresponding axis. The Galil code is as follows, see figure 4.4 for commented code. Axes A through D are configured to force control before running this program, leaving axis E and F in position control mode.

Table 4.2: gaitVaughan Marker positions

Muscle and Joint	Axis	Array Name
Hip Muscle Group	A	Hip
Hamstring Muscle Group	B	Ham
Quadriceps Muscle Group	C	Quad
Calf Muscle Group	D	Calf
Hip Joint	E	Z
Ankle Joint	F	Y

```
#GAIT             *name of gait program
N=0               *beginning incrementing at 0
PT1,1,1,1         *sets the program so that the first 4 axis to will move onto the next array point
                   even if the first point hasn't been reached
#LOOP             *array reading loop
PAA=(HIP[N])      *sets the actuators to pull at an absolute force with each loop
PAB=(HAM[N])
PAC=(QUAD[N])
PAD=(CALF[N])
JGE=Zvel[N]       *sets the velocity for the joint motion
JGF=Yvel[N]
BGE               *begin motion for joint motion
BGF
WT 10             *wait 10ms
N=N+1             *increment
JP #LOOP,N<125
EN                *end program
```

Figure 4.4: Commented Galil Code

Chapter 5

Results and Discussion

5.1 Anybody Results

The EMG output from both Anybody Software gait models; gaitUniMiami and gaitVaughan are compared with published data from Vaughan *et al.* to ensure the activity values are comparable for the measured EMG profiles [49]. Below are three muscle comparisons to show the relationship between the Anybody model output, both gaitUniMiami and gaitVaughan, to actual EMG readings, see figure 5.1, 5.2, 5.3. These show good activation tracking, which means that the muscle force output from the Anybody model can be used as realistic muscle profiles for gait.
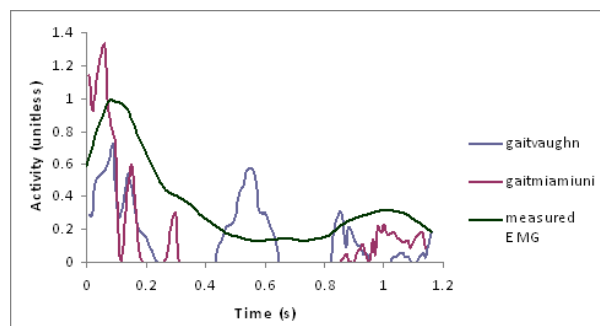
Figure 5.1: Gluteus Maximus EMG comparison
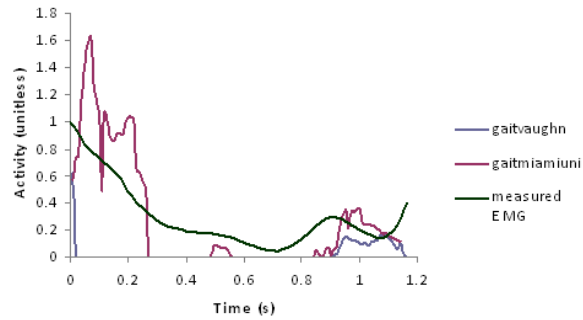
Figure 5.2: Hamstring EMG comparison
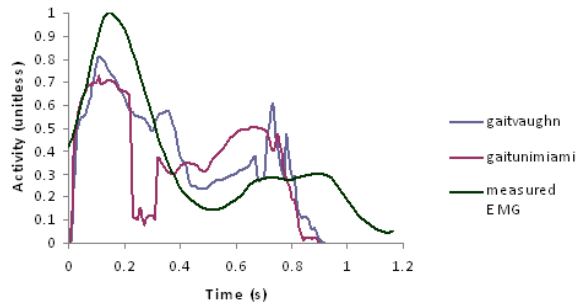
Figure 5.3: Rectus Femoris EMG comparison

All the muscle profiles from the Anybody Software were extracted. In total, 42 profiles account for the lower extremity in the Anybody model. See figure 5.4 for the combined output of all muscles. Only nine muscles are considered influential to the knee motion along with the hip moment, so not all 42 muscle profiles are needed in the simulator. As described in section 4.1.2, these muscle profiles are combined

45

into the four resultant muscle groups. See Appendix E for the array output which is used in the program for gait. See figure 5.5 for the four muscle group profiles and figure 5.6 for the joint motions.
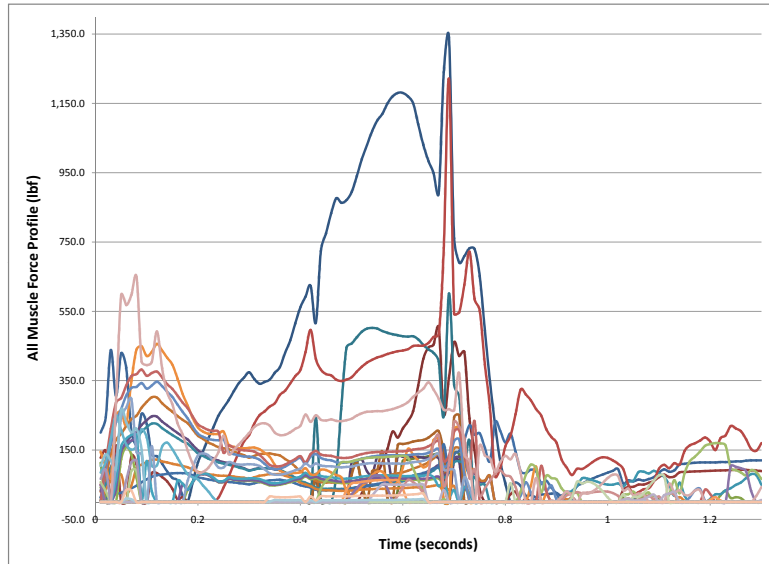
Figure 5.4: All Muscle Profiles from Anybody Software

5.2 Simulation

Comparing the results of the gait program to the load cell data shows that the simulator performs very well. Figure 5.7 shows the comparison of the load cell readings to the Anybody Software output and figure 5.8 shows the comparison of how far the joint actually travel to what the program requested. A regression coefficient study was done, see table 5.1 for the obtained results. Since the labview output does not occur every 10ms, comparing point to point between desired and actual motions is difficult. In order to perform linear regression, linear interpolation between data points from the load cell output was used. It was then possible to sample "data points", i.e. interpolated values at 10ms intervals, which allowed for a simple comparison to the Anybody model results. This analysis shows that 5 of the 6 axes perform very, but that the hamstring axis produced greater error. See Appendix F for graphs comparing the labview data, interpolated values, and Anybody model for the regression coefficient.

The ACL strain was measured for the simple gait pattern for which there is no chance of ACL injury. The strain can be compared with published data from Zhang
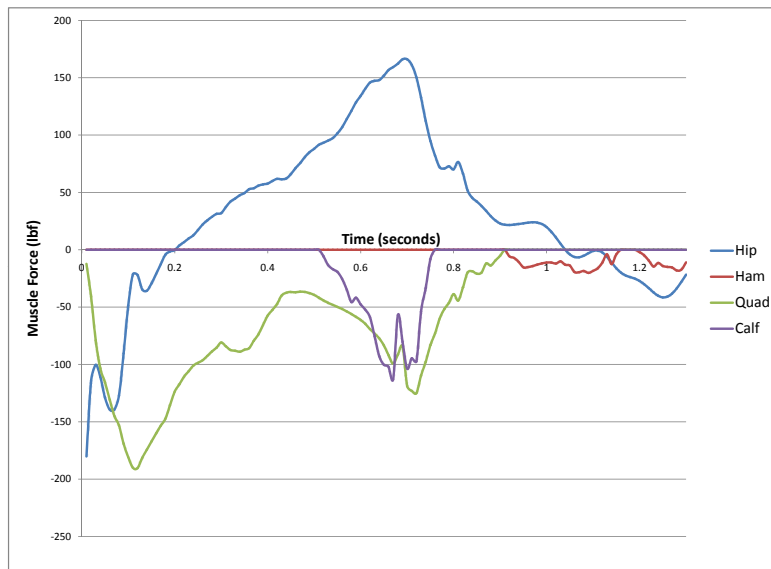
Figure 5.5: Resultant Muscle Force Profiles from Anybody Software
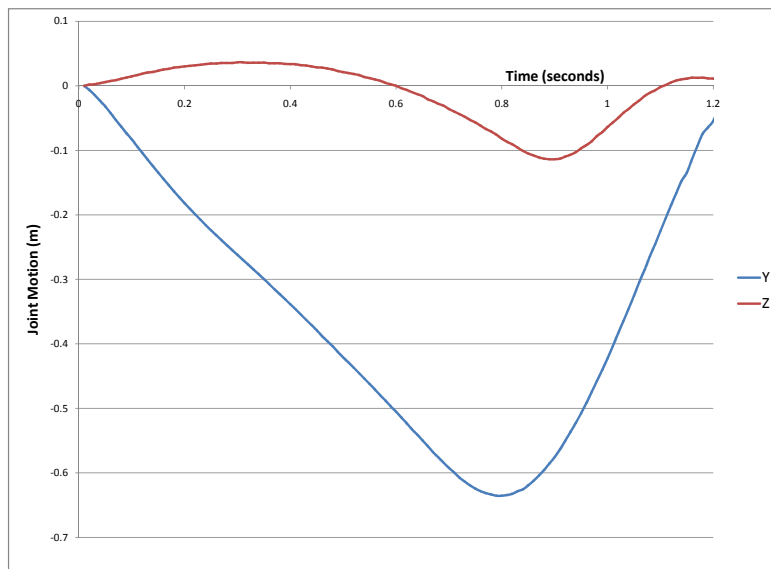
Figure 5.6: Position of the Z and Y axis' of the Joint Motion during Gait

47
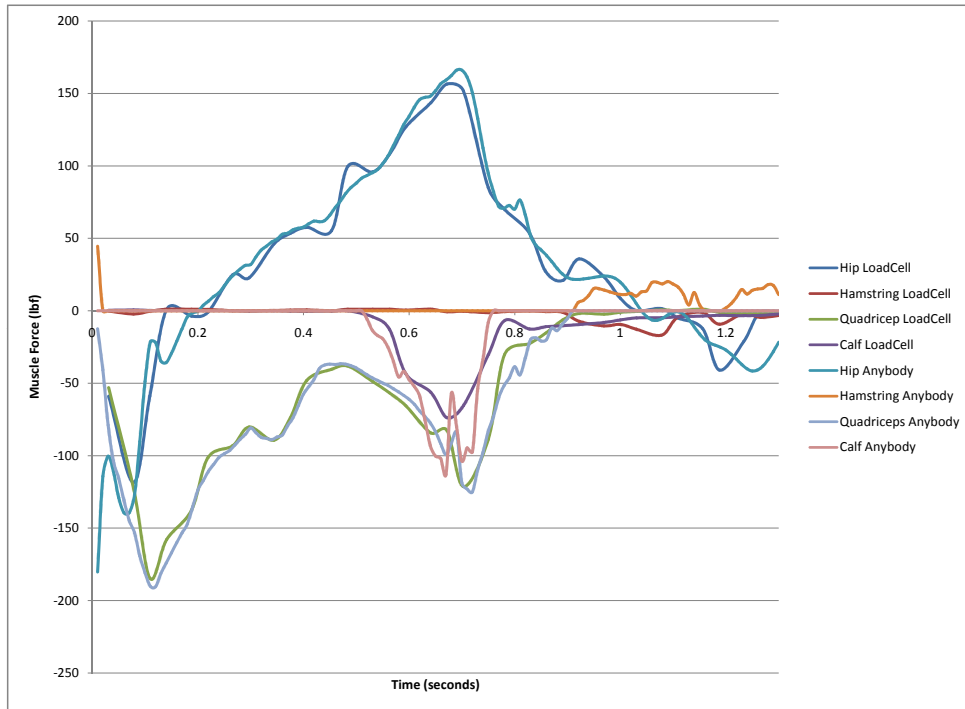
Figure 5.7: Comparison of the Muscle Force

Table 5.1: Regression Coefficient Values for each Axis

Actuator	R^2
Hip	0.929
Hamstring	0.592
Quadriceps	0.968
Calf	0.823
Ankle Motion (Y)	0.935
Hip Motion (Z)	0.96

et al. to see if the ACL is acting naturally, to ensure the DVRT works properly, and verify the attachment to the ACL [56]. Looking at the comparison closely the patterns don't seem to match well, however relative overall strain the ACL can endure, the difference is small over the whole range of 40% to 45% [50]. See figure 5.9 for comparison.
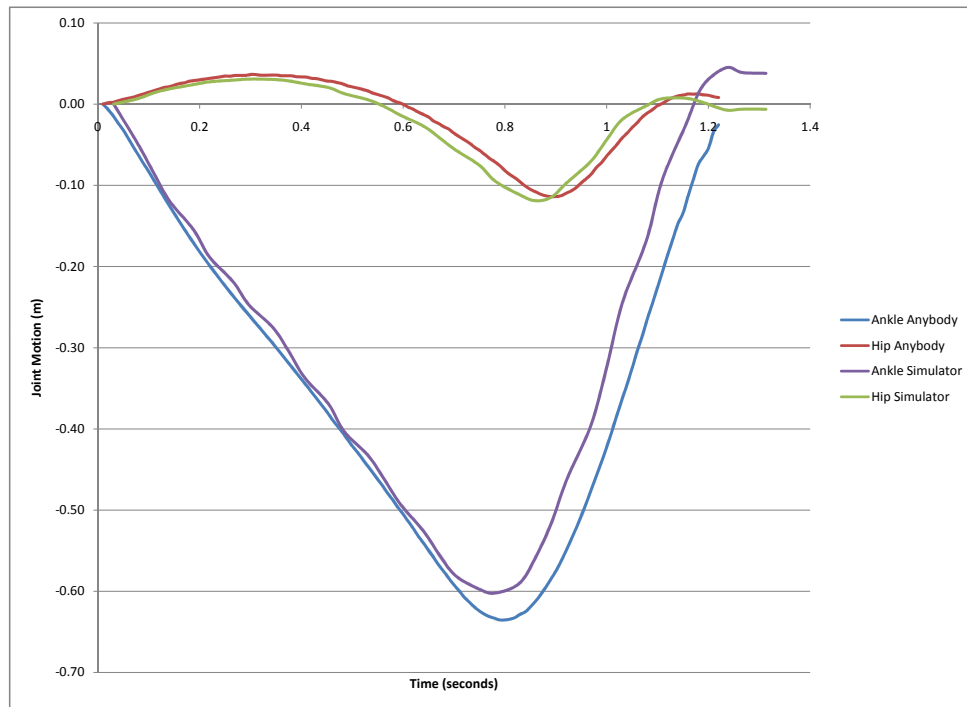
Figure 5.8: Comparison of the Joint Motion

5.3 Discussion

All six axes compare very well from input to output values, and this shows how
well the simulator resembles physiological motion for simple gait. The joint motion
compared to the motion calculated from the Anybody model shows that the velocity
assumption made in the gait program works very well. This is helpful since using
this assumption produces a smoother profile than that obtained when the motion
was programmed using only position commands. The muscle load cell readings
track closely to the Anybody model muscle profiles. Step by step comparison using
the linear interpolation technique described above, shows the axes followed the
programmed array of both muscle forces and joint velocities well. The regression
coefficient for each axis shows the simulator tracks very closely, with the exception
of the hamstring. The R^2 value is quite low, 0.592, however a closer look at the
graph in figure 5.10, the average of the graph of both the load cell reading and the
Anybody model profile are quite close, but with the rapidly fluctuating profile from
the Anybody model the actuator had difficulties following exactly.

Comparing the ACL strain to the published values, some discrepancy is evident
on a small scale. However, the range in which the difference occurs is between 1.5%
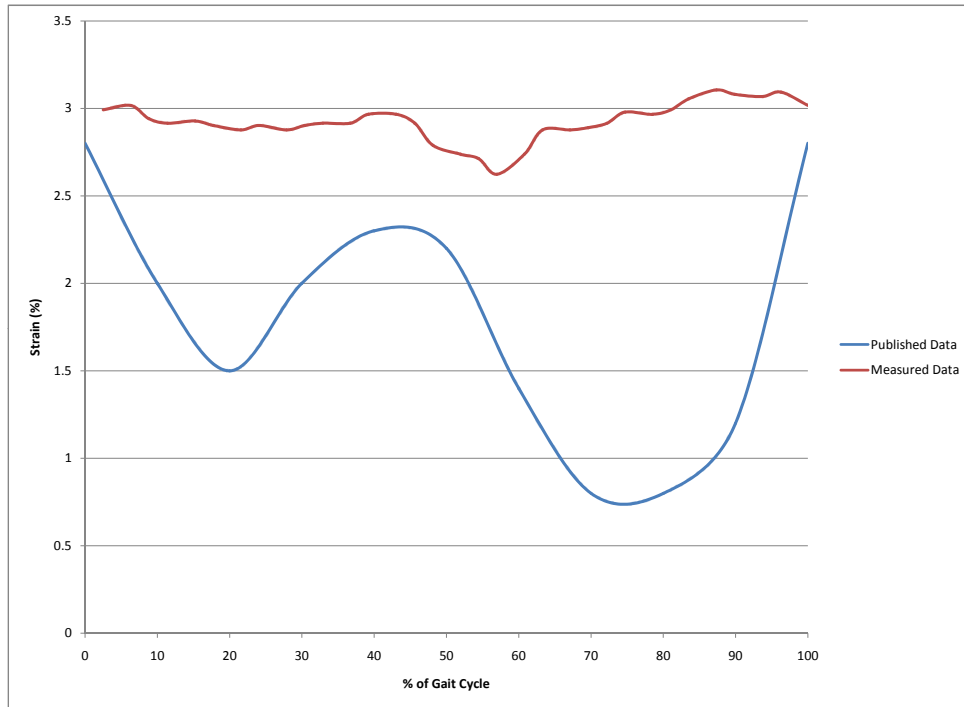
Figure 5.9: Comparison of Published Strain and Measured Strain

and 3.0% strain, where published ACL strain at injury occurs between 40% and 45% during drop landing [50]. This implies that even though the strain during gait is not directly the same as the published data, it is within the same range of strain and overall the difference is only 3.33% of the total strain the ACL can see before rupture.

The differences in the ACL strain between the Zhang *et al.* values and this simulator are most likely due to the apparatus setups and specimen preparations. The knee specimen for the Zhang *et al.* simulator has all the soft tissue on, including the skin. The muscle influence during the gait was obtained from string that was sutured to several muscles through the skin, thereby applying a tension based on muscle cross-sectional area. The motion in the knee is from the tibia, with the femur fixed. This is in contrast to the current simulator, the movement of which is influenced from both the hip and ankle. Influence of all out of plane motion is controlled from the tibia mount so that there are no natural out of plane motions. Additionally, the ground reaction force doesn't seem to be present in the Zhang simulator, which would cause a difference between the strain readings. However, there are two similarities however between these simulators which allow the comparison to have merit. The gait cycle for both are roughly the same length,

50
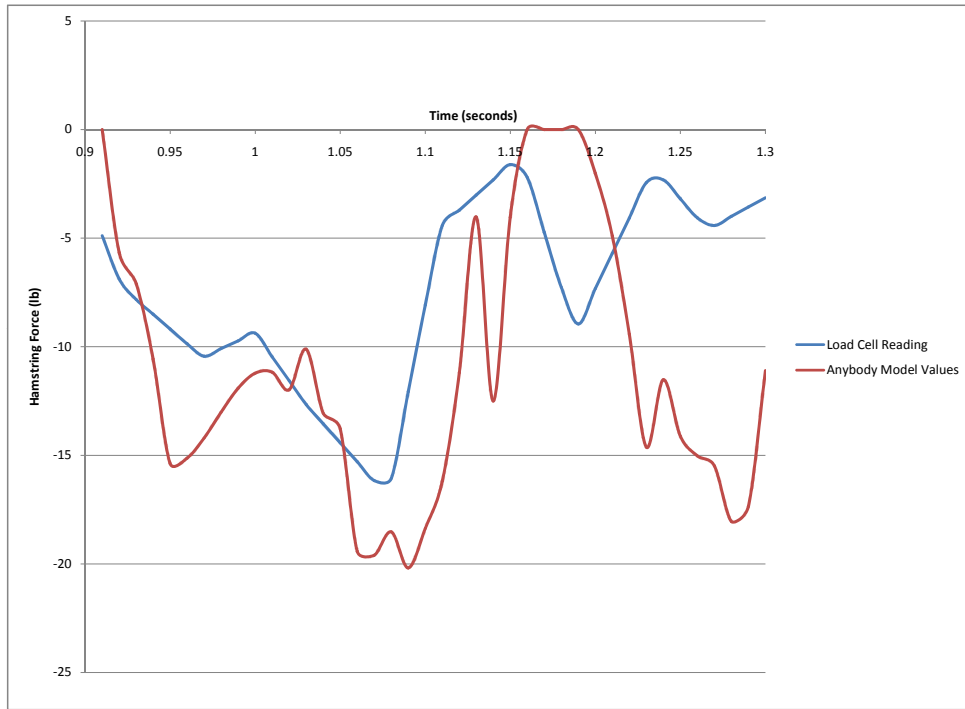
Figure 5.10: Hamstring Muscle Comparison between Load Cell Reading and Anybody Mode Results

the Zhang simulator takes 1.23 sec and this simulator takes 1.3 seconds. Also the same Microstrain DVRT was used for measuring the ACL strain. The differences most likely account for the slight difference between the two strain values. Finally, Zhang *et al/.* took several data from 30 cadaver knees each tested on 13 gait cycles. This simulator only used one trial to achieve validation. Finally measuring the DVRT while mounted on the ACL is challenging as it is difficult to measure inside the knee while it is at full extension, slight flexion in the knee is needed to get a measuring tool inside. This may distort the actual ACL strain slightly.

Since the actuators are capable of much higher speed and forces, analyzing the high-risk motions should work very well. This will allow ACL injury research to make huge advances in understanding how and why the ACL is injured.

Two major assumptions were made in the design of this simulator. First, it was assumed that the gait only occurs in the sagittal plane, with no out of plan motion. Second, several muscles were grouped together, reducing the number of actuators required and allowing the simulation to be less complex. These assumptions are both intended to simplify the simulator without sacrificing accuracy of realistic

physiological motion.

One major problem encountered during testing was the muscle attachment site of the calf muscle. Initially a single cable was put medially/laterally through the femoral condyles, similar to the hamstring muscle insertion in the tibia and in figure 5.11. When the gait simulation was activated the cable pulled out of the bone, shearing through femur, see figure 5.12. Next, the cable insertion was drilled anteriorly/posteriorly through the femur, this time with two cables as seen in figure 5.11 to split the force between them. Again when the simulation was run the cables pulled out. When the bone was analyzed after the simulations, it was observed that the bone was not in an ideal condition to begin, having minimal cortical (strong outside ring of bone structure) bone to withstand the cable force. The metal strip with the cable connection around the femur is the solution to this problem and works very well as it distributes the forces over a much larger area.
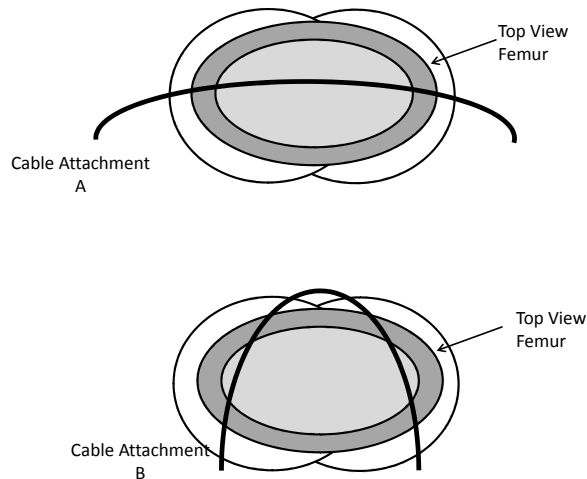
Figure 5.11: Different Failed Calf Muscle Cable Insertion Designs

Gait was the only motion used for validation, because it has readily available data and is a rather slow, simple motion. For further validation, other motions such as cycling and stair climbing, can be used. These other two motions have available data on ACL strain from other studies and Anybody Software has published models for them making the muscle and joint data easily accessible. Completing validation with these two additional motions would further validate that this simulator can accommodate all sagittal plane motions.

This simulator has certain features which make it a very realistic simulator, as described above. However, there are some limitations to consider. All motion is
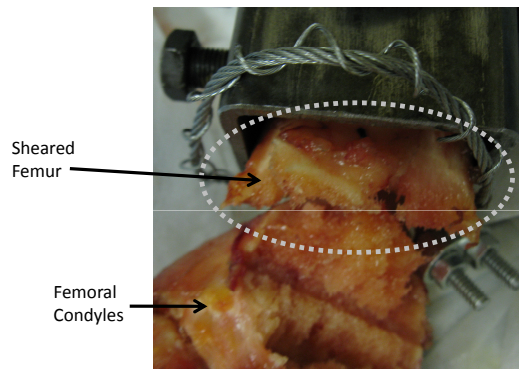
Figure 5.12: Broken Femur from Calf Muscle Insertion Cable

confined to the sagittal plane currently, and so all coronal plane motions are currently ignored. The artificial restraint on the hip and ankle is currently not reusable between simulations. A more realistic restraint, such as a spring or re-useable rubber tubing with similar elastic properties to the actual ligaments could replace the current restraint system. The muscle insertion locations are not ideal, since their mounting point is determined by the capability to attach the cable securely without chance of pull-out, so that the average insertion location is sacrificed. The Anybody Software outputs the muscle profiles, however these values are the 'best guess' values. The assumption made in the program also says that when each muscle is used in the model it is instantaneously activated. This is not a natural behaviour of human muscle, which has ramped activation.

This simulator has several branches it can be useful in other than researching ACL injury causes. It can be useful for surgical reconstruction of the ACL. The simulator can be used to test how different surgical techniques work and which are better for strength and reliability. A second use is for brace design, for both validating which brace is best but also for improving on current designs. Studies have been done to test knee braces, however they are limited to comparing different attributes, such as patients confidence in playing sports with it, to validate how well they are working.[6] This simulator is ideal for mounting a knee brace and testing how it affects the strain in the ACL.

As a summary, this simulator is a significant improvement over current simulators. There is certainly room for improvement, however this simulator can make significant contributions towards ACL injury research in the current state.

Chapter 6

Conclusion and Recommendation

6.1 Conclusion

The aim of the simulator was too create a simulated physiological reaction at the knee during different dynamic motions. Four muscle groups are attached to mimic the nine influential muscles which crossover the knee providing motion and joint stability also mimicking the hip moment. A gait step was used as the validation, keeping forces low and movements slower for initial testing.

The Anybody Software shows very good muscle profile outputs when comparing EMG activation profiles. This is a very helpful tool to the simulator as it allows the muscle contribution to be physiologically correct and dynamic, adding a crucial part of this simulators improvement over others.

The muscle tracking and joint motion turned out to follow very well. With only the hamstring not having a reasonable regression coefficient, however looking at the average of both curves they match quite well. The joint motion was very smooth with the velocity assumption and followed the required profile very well. The entire motion was very smooth and resembled a gait step. The data collection method is very accurate for capturing the load cell and DVRT data in time with the motion. From this data the ACL strain recorded seemed to match the range of the published ACL strain during gait well.

Overall, the simulator shows very good validation with simple gait. The actuators were purchased with much higher speed and force capabilities, it can be assumed this simulator will work great for high-speed, high-risk motions. This simulator will be capable of improving and adding to the research for ACL injuries.

6.2 Recommendation

There are a few recommendations for future development of the simulator. A few points to improve on the sagittal plane motion along with increasing the simulator

to 3D motion and further validation studies.

6.2.1   Design

The design works quite well so for the sagittal plan motion. A few simple recommendations can be put forward for immediate changes, i.e. further internal/external rotation stabilization. The joint, hip and ankle DOF allows a lot of internal/external rotation and abbduction/adduction which for the slower gait speeds works, however further dynamic stabilization might be helpful for faster motions.

To modify the simulator to incorporate 3D motion, a third axis, the X axis is required. This will require a joint motion actuator in the 3rd direction. A much smaller actuator is needed compared to the Y and Z axis as the medial/lateral motion is much smaller with reduced forces.

6.2.2   Anybody Software

The Anybody Model requires some further work to calculate the muscle profiles during the three high-risk basketball maneuvers for the kinematic trials completed. Further investigation of the programming for the software to understand how to incorporate the high-risk motions into the model is recommended.

6.2.3   Data Collection

The Labview program does an excellent job of collecting all the data required to analyze the components, load cells and DVRT, in the simulator. There are a large number of components needed to be monitored; 4 Omega load cells, 6 channels of the 3D Burtec load cell, position monitoring of the joint actuators, and the DVRT signal. This causes the Labview program to run each cycle of data collection at no faster than 31ms cycles. It would be helpful to find a method to speed up the collection process so that it can be monitored with the 10ms interval of the program. This would help with comparison to the input values to ensure complete similarity between them.

6.2.4   Further Validation and Testing

Running the gait simulation in a cyclic motion would be helpful for validation to ensure the simulator maintains it's reliability seen in the single gait trial. After that, using more motions such as cycling and stair climbing will allow further validation into the versatility of the simulator. These motions are ideal as they have published ACL strain data to compare with, also the Anybody Software has published models for both these motions providing easily accessible joint motions and muscle profiles.

Once the Anybody Model for jump landing is completed, testing can begin on actual ACL injuries during high-risk motions.

Appendices

Appendix A

RSA Actuator Specification

RSA/RSM32 Series
ACME SCREW SPECIFICATIONS

RSA32 ACME SCREW CRITICAL SPEED AND PV LIMITS

CRITICAL SPEED WITH 0.75" 1TPI ENGLISH ACME SCREW

MAX THRUST*: 300 LB
RSA32 SN01
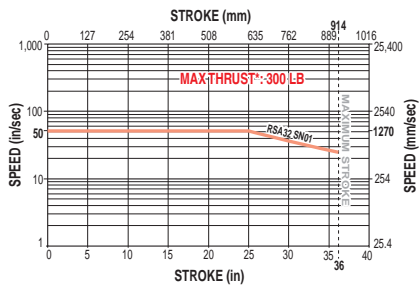
PV LIMITS: 0.75" 1TPI ENGLISH ACME SCREW

RSA32 SN01

CRITICAL SPEED WITH 0.75" 2TPI ENGLISH ACME SCREW

MAX THRUST*: 300 LB
RSA32 SN02
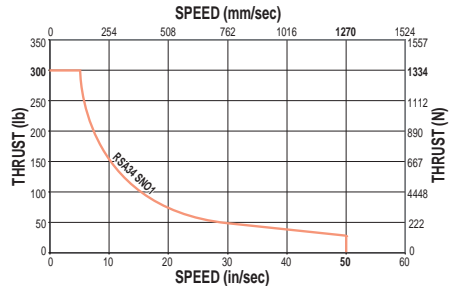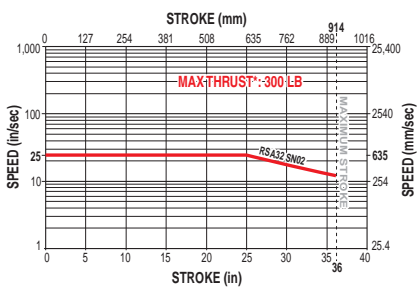
PV LIMITS: 0.75" 2TPI ENGLISH ACME SCREW

RSA32 SN02
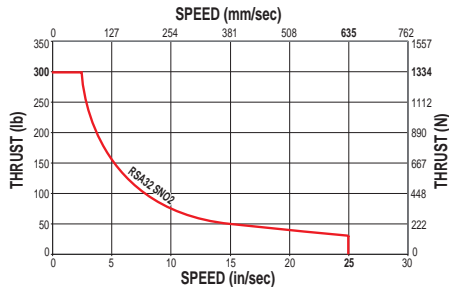
CRITICAL SPEED WITH 0.75" 10TPI ENGLISH ACME SCREW

MAX THRUST*: 2500 LB
RSA32 BZ10
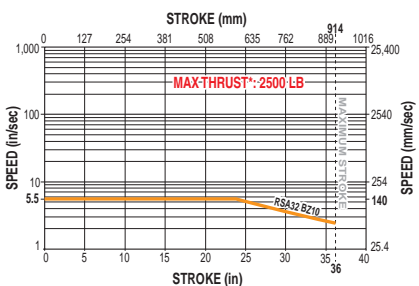
PV LIMITS: 0.75" 10TPI ENGLISH ACME SCREW

RSA32 BZ10
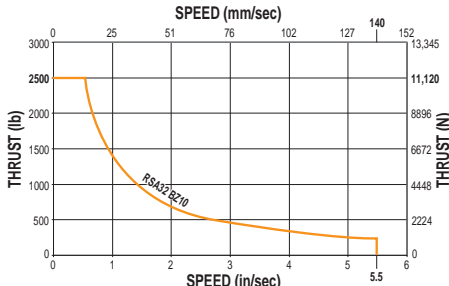
SN = Solid Nut   BZ= Bronze Nut

⚠ *** Maximum thrust is the maximum continuous dynamic thrust subject to Thrust x Velocity limitation.**

PV LIMITS: Any material which carries a sliding load is limited by heat buildup. The factors that affect heat generation rate in an application are the pressure on the nut in pounds per square inch and the surface velocity in feet per minute. The product of these factors provides a measure of the severity of an application.

$$\left(\frac{\text{Thrust}}{\text{(Max. Thrust Rating)}}\right) \times \left(\frac{\text{Speed}}{\text{(Max. Speed Rating)}}\right) \leq 0.1$$

$$\left(P\right) \times \left(V\right) \leq 0.1$$

RSA/RSM32 Series

BALL SCREW SPECIFICATIONS

RSA32 BALL SCREW CRITICAL SPEED AND LIFE CALCULATIONS

CRITICAL SPEED WITH 0.75" 2TPI ENGLISH BALL SCREW
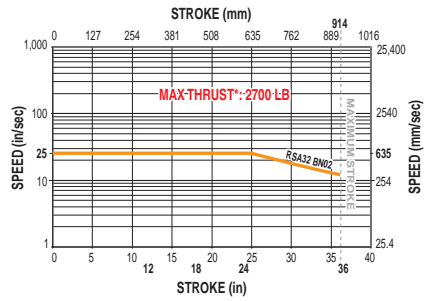
LIFE CALCULATION: 0.75" 2TPI ENGLISH BALL SCREW
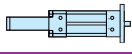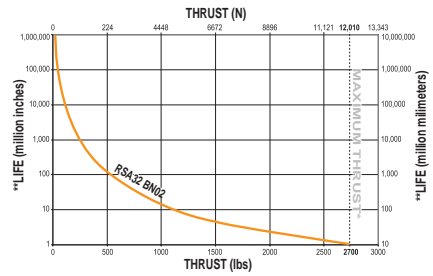
ROD SCREW

RSA/RSM32 Series
• Ball screw critical speed and life calculations

CRITICAL SPEED WITH 0.75" 5TPI ENGLISH BALL SCREW
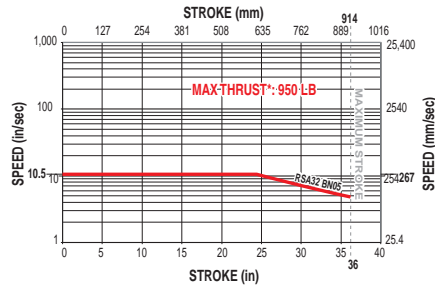
LIFE CALCULATION: 0.75" 5TPI ENGLISH BALL SCREW
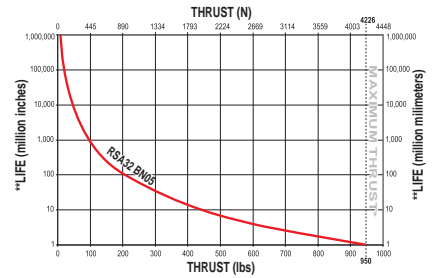
BN = Ball Nut

⚠️ ** Maximum thrust reflects 90% reliability for 1 million linear inches of travel.*

**Life indicates theoretical maximum life of screw only, under ideal conditions and does not indicate expected life of actuator.

Appendix B

Macron Actuator Specification

MACRON Product	PULLEY	BELT	BEAM OPTION	CART WEIGHT/LBS
MACRON PSC-28	28	12H	28×38	.35 (5.6oz)*
MACRON Mini 6-28	28	12S, 12H	28 x n	1.156*
MACRON 6	40	**25S**	**40 x n**	3.406*
MACRON 6 Z	40	25S	40 x n	N/A
MACRON 135	40	25S, 25H	40 x 80 Track	1.594*
MACRON 14	40 or 80	25S, 25H, 50S, 50H	40/80 x n	7.811*
MACRON 14 Z	40	25S, 50S	40/80 x n	N/A
MACRON 14 H	40 or **80**	25, **50** (S,**H**)	40/**80 x n**	12.00*
MACRON Rail	28, 40, 80	12, 25, 50 (S,H)	40/80 x n	App. Specific
MACRON Rail All Stainless	28, 40, 80 28	12, 25, 50 (S,H)	App. Specific	App. Specific
MACRON Single Belt Drive 12	28	12H	28 x n	N/A
MACRON Single Belt Drive 25	40	25S, 25H	40/80 x n	N/A
MACRON Single Belt Drive 50	40	50S, 50H	80 x n	N/A
MACRON Single Belt Drive 50 H	80	50H	80 x n	N/A
MACRON Dual Independent Belt Drive	40	25S, 25H	80 x n	N/A

S = Standard, H = Heavy

n = See MacFRAME Section for Extrusion Options

Note: Cart Type Determines Actuator Style
* Weight shown is for standard cart only.

Contact factory for other cart weights.

SHAFTED PULLEY ASSEMBLY Options
A = Single Shafted Pulley

B = Double Shafted Pulley
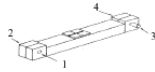
EXAMPLE (in bold)	Product	PULLEY	BELT WIDTH	BEAM OPTION	SHAFT & LOCATIONS
	6	40	25S	40×80	A1
	14H	80	50H	80×98	A3

Pulley Specifications

Note: All Shafted Pulleys are Machined as one piece from a solid bar of stress proof steel

	Belt Width						Pulley Weight		
'A' Dim	12mm	25mm	50mm	Teeth	Pitch	Travel/Revolution	Shafted	Idler	Double Shafted
28mm	x			21	5mm	105mm (4.134 in)	4.7 oz	4.3 oz	5.4 oz
40mm		x		15	10mm	150mm (5.906 in)	11.3 oz	7.7 oz	17 oz
40mm			x	15	10mm	150mm (5.906 in)	28.4 oz	26.4 oz	31.5 oz
80mm			x	28	10mm	280mm (11.020 in)	105 oz	92.0 oz	119.0 oz

Pulley Diameter = Travel/Revolution divided by 3.1415

All Belts are made of Polyurethane material and steel cords

Belt and Pulley Assembly

A Dim = 28, 40, 80 mm

BELT TENSIONING TOOL
Belt can be adjusted to a +/- 5 lbs-in range for smooth motion using Macron Belt Tensioning Tool

▶ BUY   ORDER ON-LINE

Belt Tensioning Procedures
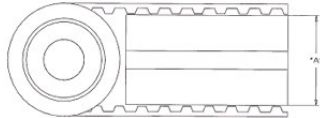
Recommended Running Load

Using Safety Factor of 4

		Belt Width		
		12mm	25mm	50mm
Belt Type	S	NA	1945 N 437 Lbs	5118 N 1150 Lbs
	H	1282 N 288 Lbs	4570 N 1027 Lbs	12015 N 2700 Lbs

Belt Weight

	Belt Width	
12mm	25mm	50mm

Belt Tension 'Recommended Max Preload Range'
Belt can be adjusted to a +/- 5 lbs-in range

		Belt Width		
		12mm	25mm	50mm
Belt Type	S	NA	890 N 200 Lbs	1335 N 300 Lbs
	H	445 N 100 Lbs	1335 N 300 Lbs	1780 N 400 Lbs

Ultimate Tensile Strength For Belts

	Belt Width	
12mm	25mm	50mm

Belt Type	S	NA	.076 Lb/Ft .114 Kg/M	.160 Lb/Ft .235 Kg/M
	H	.029 Lb/Ft .043 Kg/M	.121 Lb/Ft .181 Kg/M	.226 Lb/Ft .336 Kg/M

Belt Type	S	NA	7787 N 1750 Lbs	20470 N 4600 Lbs
	H	5117.5 N 1150 Lbs	18280 N 4108 Lbs	48040 N 10800 Lbs

S=Standard, H=Heavy, N=Newtons

Belt And Pulley Assembly Dimensional Drawing

28-12 Pulley Assembly – (Single and Double Shafted)
28-12C Pulley Assembly – (Single and Double Shafted)
28-12H Pulley Assembly – (Single and Double Shafted)
40-25 Pulley Assembly – (Single and Double Shafted)
40-50 Pulley Assembly – (Single and Double Shafted)
80-50 Pulley Assembly – (Single and Double Shafted)
80-50M Pulley Assembly – (Single and Double Shafted)

Comments (0) View Related Posts In: **Product Specifications**

Privacy Policy | Disclaimer

MACRON DYNAMICS, INC.
100 Phyllis Drive
Croydon, PA 19021
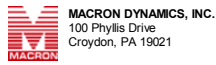
Motion Solutions Since 1987

1-800-MACRON-1 (1-800-622-7661)
Phone: 215-443-8888
Fax: 215-443-0981
E-mail Macron

Appendix C

Danaher Motion Motor Specification

Performance Data - AKM4x Frame

SHOWN WITH "C"
CONNECTOR OPTION

SHOWN WITH "D"
CONNECTOR OPTION

SHOWN WITH "M" OR "P"
CONNECTOR OPTION

AKM41 (103.1[4.06])
AKM42 (132.1[5.20])
AKM43 (161.1[6.34])
AKM44 (190.1[7.48])
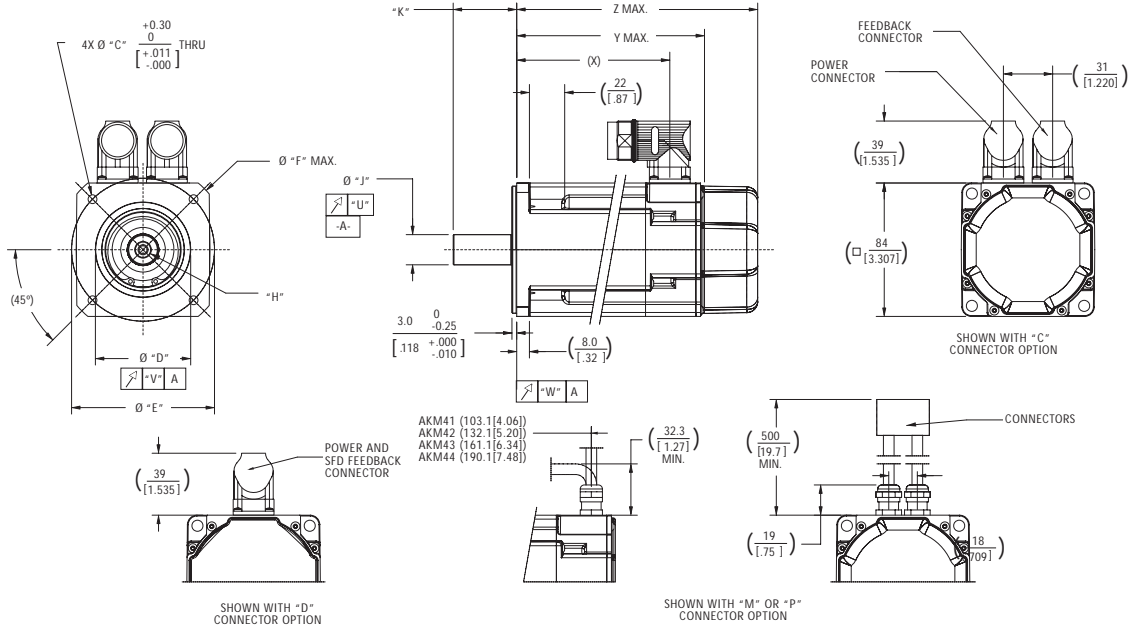
MOUNTING CODE	"C"	"D"	"E"	"F"	"H"	"J"	"K"	"L"	"M"	"N"
AC	7 [.276]	80 +0.012/-0.007 [3.1496 +.0004/-.0002] j6	100 [3.937]	–	D M6 DIN 332	19 +0.015/+0.002 [.7480 +.0006/.0001] k6	40.0 [1.57]	–	–	–
AN	7 [.276]	80 +0.012/-0.007 [3.1496 +.0004/-.0002] j6	100 [3.937]	–	D M6 DIN 332	19 +0.015/+0.002 [.7480 +.0006/.0001] k6	40.0 [1.57]	–	–	–
BK	5.54 [.218]	73.025 0/-0.051 [2.8750 +.0000/-.0002]	98.43 [3.875]	–	–	15.875 0/-0.013 [.6250 +.0000/-.0005]	52.40 ± 0.79 [2.063 ± .031]	17.92 0/-0.43 [.706 +.000/-.017]	4.762 0/-0.050 [.1875 +.0000/-.0020]	34.93 ± 0.25 [1.375 ± .010]
CC	5.54 [.218]	60 +0.012/-0.007 [2.3622 +.0004/-.0002] j6	90 [3.543]	109 [4.291]	D M6 DIN 332	19 +0.015/+0.002 [.7480 +.0006/.0001] k6	40.0 [1.57]	–	–	–
CN	5.54 [.218]	60 +0.012/-0.007 [2.3622 +.0004/-.0002] j6	90 [3.543]	109 [4.291]	D M6 DIN 332	19 +0.015/+0.002 [.7480 +.0006/.0001] k6	40.0 [1.57]	–	–	–
EK	5.54 [.218]	73.025 0/-0.051 [2.8750 +.0000/-.0020]	98.43 [3.875]	–	–	12.700 0/-0.013 [.5000 +.0000/-.0005]	31.75 ± 0.25 [1.250 ± .010]	14.09 0/-0.43 [.555 +.000/-.017]	3.175 0/-0.050 [.1250 +.0000/-.0020]	19.05 ± 0.25 [.750 ± .010]

MOUNTING CODE	"P"	"R"	"S"	"T"	"U"	"V"	"W"
AC	21.5 0/-0.13 [.846 +.000/-.005]	6 0/-0.03 [.236 +.000/-.001] N9	4.00 [1.57]	32 0/-0.30 [1.260 +.000/-.012]	0.040 [.0015]	0.080 [.0031]	0.080 [.0031]
AN	–	–	–	–	0.040 [.0015]	0.080 [.0031]	0.080 [.0031]
BK	–	–	–	–	0.051 [.0020]	0.10 [.004]	0.10 [.004]
CC	21.5 0/-0.13 [.846 +.000/-.005]	6 0/-0.03 [.236 +.000/-.001] N9	4.00 [1.57]	32 0/-0.30 [1.260 +.000/-.012]	0.040 [.0015]	0.080 [.0031]	0.080 [.0031]
CN	–	–	–	–	0.040 [.0015]	0.080 [.0031]	0.080 [.0031]
EK	–	–	–	–	0.051 [.0020]	0.10 [.004]	0.10 [.004]

(X)	Y MAX.	Z MAX. (W/ BRAKE)	MODEL
96.4 [3.80]	118.8 [4.68]	152.3 [6.00]	AKM41
125.4 [4.94]	147.8 [5.82]	181.3 [7.14]	AKM42
154.4 [6.08]	176.8 [6.96]	210.3 [8.28]	AKM43
183.4 [7.22]	205.8 [8.10]	239.3 [9.42]	AKM44

Dimensions are in mm [inches].
Product designed in metric.
English conversions provided for reference only.

22
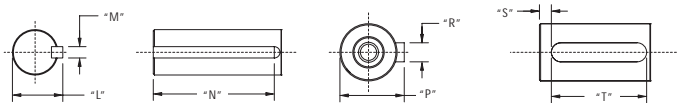
Performance Data - AKM4x Frame

AKM4x - Up to 640 VDC

See system data beginning on page 8 for typical torque/speed performance.

PARAMETER	Tol	SYMBOL	UNITS	AKM41 C	AKM41 E	AKM41 H	AKM42 C	AKM42 E	AKM42 G	AKM42 J	AKM43 E	AKM43 G	AKM43 K	AKM44 E	AKM44 G	AKM44 J
Max Rated DC Bus Voltage	Max	V_{bus}	Vdc	640	640	320	640	640	640	320	640	640	320	640	640	640
Continuous Torque (Stall) for	Nom	T_{cs}	N-m	1.95	2.02	2.06	3.35	3.42	3.53	3.56	4.70	4.80	4.90	5.76	5.88	6.00
ΔT winding = 100°C ①②⑦⑧⑨			lb-in	17.3	17.9	18.2	29.6	30.3	31.2	31.5	41.6	42.5	43.4	51.0	52.0	53.1
Continuous Current (Stall) for	Nom	I_{cs}	A_{rms}	1.46	2.85	5.60	1.40	2.74	4.80	8.40	2.76	4.87	9.60	2.9	5.0	8.8
ΔT winding = 100°C ①②⑦⑧⑨																
Continuous Torque (Stall) for	Nom	T_{cs}	N-m	1.56	1.62	1.65	2.68	2.74	2.82	2.85	3.76	3.84	3.92	4.61	4.70	4.80
ΔT winding = 60°C ②			lb-in	13.8	14.3	14,6	23,7	24.2	25.0	25.2	33.3	34.0	34.7	40.8	41.6	42.5
Max Mechanical Speed ⑤	Nom	N_{max}	rpm	6000	6000	6000	6000	6000	6000	6000	6000	6000	6000	6000	6000	6000
Peak Torque ①②	Nom	T_p	N-m	6.12	6.28	6.36	11.1	11.3	11.5	11.6	15.9	16.1	16.3	19.9	20.2	20.4
			lb-in	54.2	55.6	56.3	98.8	99.7	102	103	141	142	144	176	179	181
Peak Current	Nom	I_p	A_{rms}	5.8	11.4	22.4	5.61	11.0	19.2	33.7	11.0	19.5	38.3	11.4	20.0	35.2
75VDC Rated Torque (speed) ①②⑦⑧⑨⑩		T_{rtd}	N-m	-	-	1.99	-	-	-	-	-	-	-	-	-	-
			lb-in	-	-	17.6	-	-	-	-	-	-	-	-	-	-
Rated Speed		N_{rtd}	rpm	-	-	1000	-	-	-	-	-	-	-	-	-	-
Rated Power (speed) ①②⑦⑧⑨		P_{rtd}	kW	-	-	0.21	-	-	-	-	-	-	-	-	-	-
			Hp	-	-	0.28	-	-	-	-	-	-	-	-	-	-
160VDC Rated Torque (speed) ①②⑦⑧⑨⑩		T_{rtd}	N-m	-	1.94	1.86	-	-	-	3.03	-	-	4.08	-	-	-
			lb-in	-	17.2	16.5	-	-	-	26.8	-	-	36.1	-	-	-
Rated Speed		N_{rtd}	rpm	-	1200	3000	-	-	-	3000	-	-	2500	-	-	-
Rated Power (speed) ①②⑦⑧⑨		P_{rtd}	kW	-	0.24	0.58	-	-	-	0.95	-	-	1.07	-	-	-
			Hp	-	0.33	0.78	-	-	-	1.28	-	-	1.43	-	-	-
320VDC Rated Torque (speed) ①②⑦⑧⑨⑩		T_{rtd}	N-m	1.88	1.82	1.62	-	3.12	2.90	2.62	4.24	4.00	2.62	5.22	4.90	3.84
			lb-in	16.6	16.1	14.3	-	27.6	25.7	21.1	37.5	35.4	23.2	46.2	43.4	34.0
Rated Speed		N_{rtd}	rpm	1200	3000	6000	-	1800	3500	6000	1500	2500	6000	1200	2000	4000
Rated Power (speed) ①②⑦⑧⑨		P_{rtd}	kW	0.24	0.57	1.02	-	0.59	1.06	1.50	0.67	1.05	1.65	0.66	1.03	1.61
			Hp	0.32	0.77	1.36	-	0.79	1.42	2.00	0.89	1.40	2.21	0.88	1.38	2.16
560VDC Rated Torque (speed) ①②⑦⑧⑨⑩		T_{rtd}	N-m	1.77	1.58	-	3.10	2.81	2.35	-	3.92	3.01	-	4.80	3.76	2.75
			lb-in	15.7	14.0	-	27.4	24.9	20.8	-	34.7	26.6	-	42.5	33.3	24.3
Rated Speed		N_{rtd}	rpm	3000	6000	-	1500	3500	6000	-	2500	5000	-	2000	4000	6000
Rated Power (speed) ①②⑦⑧⑨		P_{rtd}	kW	0.56	0.99	-	0.49	1.03	1.48	-	1.03	1.58	-	1.01	1.57	1.73
			Hp	0.75	1.33	-	0.65	1.38	1.98	-	1.38	2.11	-	1.35	2.11	2.32
640VDC Rated Torque (speed) ①②⑦⑧⑨⑩		T_{rtd}	N-m	1.74	1.58	-	3.02	2.72	2.35	-	3.76	2.57	-	4.56	3.19	2.75
			lb-in	15.4	14.0	-	26.7	24.1	20.8	-	33.3	22.7	-	40.4	28.2	24.3
Rated Speed		N_{rtd}	rpm	3500	6000	-	2000	4000	6000	-	3000	6000	-	2500	5000	6000
Rated Power (speed) ①②⑦⑧⑨		P_{rtd}	kW	0.64	0.99	-	0.63	1.14	1.48	-	1.18	1.61	-	1.19	1.67	1.73
			Hp	0.85	1.33	-	0.85	1.53	1.98	-	1.58	2.16	-	1.60	2.24	2.32
Torque Constant ①	±10%	K_t	N-m/A_{rms}	1.34	0.71	0.37	2.40	1.26	0.74	0.43	1.72	0.99	0.52	2.04	1.19	0.69
			lb-in/A_{rms}	11.9	6.3	3.3	21.2	11.2	6.5	3.8	15.2	8.8	4.6	18.1	10.5	6.1
Back EMF constant ⑥	±10%	K_e	V/k$_{rpm}$	86.3	45.6	23.7	154	80.9	47.5	27.5	111	63.9	33.2	132	76.6	44.2
Resistance (line-line) ⑥	±10%	R_m	Ω	21.7	5.7	1.51	27.52	7.22	2.38	0.80	8.04	2.61	0.70	8.08	2.65	0.88
Inductance (line-line)		L	mH	66.1	18.4	5.0	97.4	26.8	9.2	3.1	32.6	10.8	2.9	33.9	11.5	3.8
Inertia		J_m	kg-cm^2	0.81			1.5				2.1			2.7		
(includes Resolver feedback) ③			lb-in-s^2	7.2E-04			1.3E-03				1.8E-03			2.4E-03		
Optional Brake Inertia		J_m	kg-cm^2	0.068			0.068				0.068			0.068		
(additional)			lb-in-s^2	6.0E-05			6.0E-05				6.0E-05			6.0E-05		
Weight		W	kg	2.44			3.39				4.35			5.3		
			lb	5.4			7.5				9.6			11.7		
Static Friction ①⑩		T_f	N-m	0.014			0.026				0.038			0.05		
			lb-in	0.12			0.23				0.34			0.44		
Viscous Damping ①		K_{dv}	N-m/k$_{rpm}$	0.009			0.013				0.017			0.021		
			lb-in/k$_{rpm}$	0.08			0.12				0.15			0.19		
Thermal Time Constant		TCT	minutes	13			17				20			24		
Thermal Resistance		R_{thw-a}	°C/W	1.04			0.89				0.78			.71		
Pole Pairs				5			5				5			5		
Heatsink Size				10″x10″x¹/₄″ Aluminum Plate			10″x10″x¹/₄″ Aluminum Plate				10″x10″x¹/₄″ Aluminum Plate			10″x10″x¹/₄″ Aluminum Plate		

Notes:
1. Motor winding temperature rise, ΔT=100°C, at 40°C ambient.
2. All data referenced to sinusoidal commutation.
3. Add parking brake if applicable for total inertia.
4. Motor with standard heatsink.
5. May be limited at some values of Vbus.
6. Measured at 25°C.

7. Brake motor option reduces continuous torque ratings by 0.12 N-m.

8. Non-Resolver feedback options reduces continuous ratings by:
   AKM41 = 0.1 N-m   AKM42 = 0.1 N-m
   AKM43 = 0.2 N-m   AKM44 = 0.3 N-m

9. Motors with non-Resolver feedback and Brake option, reduce continuous torque by::
   AKM41 = 0.22 N-m   AKM42 = 0.36 N-m
   AKM43 = 0.55 N-m   AKM44 = 0.76 N-m
10. For motors with optional shaft seal, reduce torque shown by 0.071 N-m (0.63lb-in), and increase T_f by the same amount.

Performance Data - AKM7x Frame
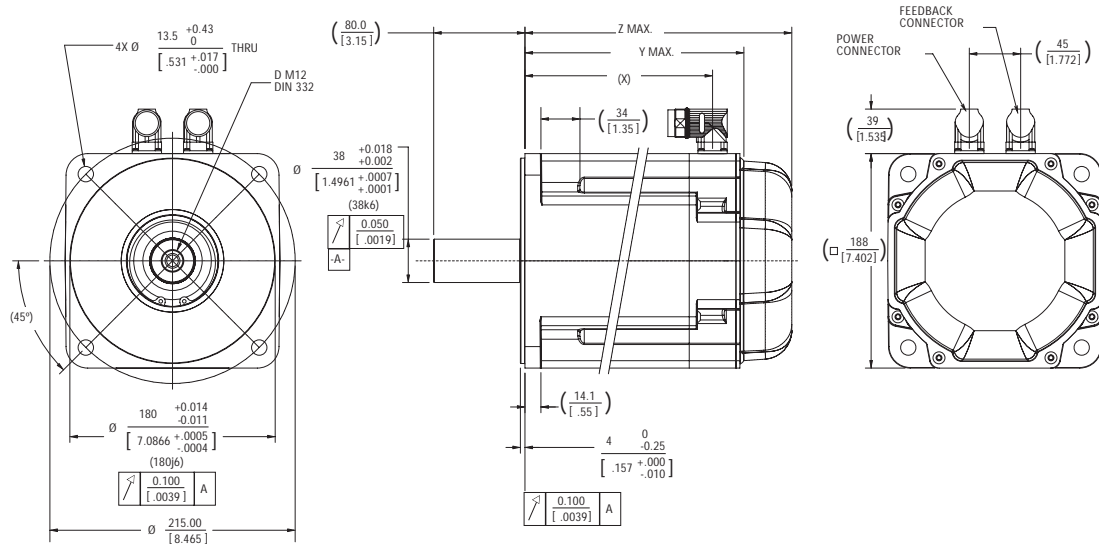
MOUNTING CODE	"T"	"U"	"V"	"W"
AC	10 $^{0}_{-0.036}$ N9 [.3937 $^{+.0000}_{-.0014}$]	41 $^{0}_{-0.29}$ [1.614 $^{+.000}_{-.011}$]	5.00 [.197]	70 $^{0}_{-0.30}$ [2.756 $^{+.000}_{-.012}$]
AN	–	–	–	–

Dimensions are in mm [inches].
Product designed in metric.
English conversions provided for reference only.

Z MAX. SINE ENCODER (NO BRAKE)	Z MAX. SINE ENCODER (W/ BRAKE)	(X)	Y MAX.	Z MAX. (W/ BRAKE)	MODEL
201.7 [7.94]	253.3 [9.97]	164.5 [6.48]	192.5 [7.58]	234.5 [9.23]	AKM72
235.7 [9.38]	287.3 [11.31]	198.5 [7.81]	226.5 [8.92]	268.5 [10.57]	AKM73
269.7 [10.62]	321.3 [12.65]	232.5 [9.15]	260.5 [10.26]	302.5 [11.91]	AKM74

Performance Data - AKM7x Frame

AKM7x - Up to 640 VDC

See system data beginning on page 8 for typical torque/speed performance.

				AKM72			AKM73		AKM74	
PARAMETER	Tol	SYMBOL	UNITS	K	M	P	M	P	L	P
Max Rated DC Bus Voltage	Max	Vbus	Vdc	640	640	640	640	640	640	640
Continuous Torque (Stall) for	Nom	T_{cs}	N-m	29.7	30.0	29.4	42.0	41.6	53.0	52.5
ΔT winding = 100°C ①②⑦⑧⑨			lb-in	263	266	260	372	368	469	465
Continuous Current (Stall) for	Nom	I_{cs}	A_{rms}	9.3	13.0	18.7	13.6	19.5	12.9	18.5
ΔT winding = 100°C ①②⑦⑧⑨										
Continuous Torque (Stall) for	Nom	T_{cs}	N-m	23.8	24.0	23.5	33.6	33.3	42.4	42.0
ΔT winding = 60°C ②			lb-in	211	212	208	297	295	375	372
Max Mechanical Speed ⑤	Nom	N_{max}	rpm	6000	6000	6000	6000	6000	6000	6000
Peak Torque ①②	Nom	T_p	Nm	79.2	79.7	78.5	113	111	143	142
			lb-in	701	705	695	997	985	1269	1253
Peak Current	Nom	I_p	A_{rms}	27.8	38.9	56.1	40.8	58.6	38.7	55.5

75VDC

Rated Torque (speed) ①②⑦⑧⑨⑩		T_{rtd}	N-m	-	-	-	-	-	-	-
			lb-in	-	-	-	-	-	-	-
Rated Speed		N_{rtd}	rpm	-	-	-	-	-	-	-
Rated Power (speed) ①②⑦⑧⑨		P_{rtd}	kW	-	-	-	-	-	-	-
			Hp	-	-	-	-	-	-	-

160VDC

Rated Torque (speed) ①②⑦⑧⑨⑩		T_{rtd}	N-m	-	-	-	-	-	-	-
			lb-in	-	-	-	-	-	-	-
Rated Speed		N_{rtd}	rpm	-	-	-	-	-	-	-
Rated Power (speed) ①②⑦⑧⑨		P_{rtd}	kW	-	-	-	-	-	-	-
			Hp	-	-	-	-	-	-	-

320VDC

Rated Torque (speed) ①②⑦⑧⑨⑩		T_{rtd}	N-m	-	-	23.8	-	34.7	-	-
			lb-in	-	-	211	-	307	-	-
Rated Speed		N_{rtd}	rpm	-	-	1800	-	1300	-	-
Rated Power (speed) ①②⑦⑧⑨		P_{rtd}	kW	-	-	4.49	-	4.72	-	-
			Hp	-	-	6.01	-	6.33	-	-

560VDC

Rated Torque (speed) ①②⑦⑧⑨⑩		T_{rtd}	N-m	25.1	23.6	20.1	33.8	28.5	43.5	39.6
			lb-in	222	209	178	299	252	385	350
Rated Speed		N_{rtd}	rpm	1500	2000	3000	1500	2400	1200	1800
Rated Power (speed) ①②⑦⑧⑨		P_{rtd}	kW	3.94	4.94	6.31	5.31	7.16	5.47	7.46
			Hp	5.29	6.63	8.46	7.12	9.60	7.33	10.01

640VDC

Rated Torque (speed) ①②⑦⑧⑨⑩		T_{rtd}	N-m	24.0	22.1	18.2	32.1	26.3	41.5	35.9
			lb-in	212	196	161	284	233	367	318
Rated Speed		N_{rtd}	rpm	1800	2500	3500	1800	2800	1400	2000
Rated Power (speed) ①②⑦⑧⑨		P_{rtd}	kW	4.52	5.79	6.67	6.05	7.71	6.08	7.52
			Hp	6.06	7.76	8.94	8.11	10.34	8.16	10.08

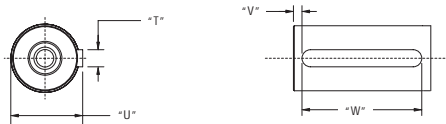|										
Torque Constant ①	±10%	K_t	N-m/A_{rms}	3.23	2.33	1.58	3.10	2.13	4.14	2.84
			lb-in/A_{rms}	28.6	20.6	14.0	27.4	18.9	36.6	25.1
Back EMF constant ⑥	±10%	K_e	V/k_{rpm}	208	150	102	200	137	266	183
Resistance (line-line) ⑥	±10%	R_m	Ω	1.22	0.64	0.33	0.68	0.35	0.85	0.43
Inductance (line-line)		L	mH	20.7	10.8	5.0	12.4	5.9	16.4	7.7
Inertia		J_m	kg-cm²		65			92		120
(includes Resolver feedback) ③			lb-in-s²		0.057			0.082		0.11
Optional Brake Inertia		J_m	kg-cm²		1.64			1.64		1.64
(additional)			lb-in-s²		1.46×10^{-3}			1.46×10^{-3}		1.46×10^{-3}
Weight		W	kg		19.7			26.7		33.6
			lb		43.4			58.8		74.0
Static Friction ①⑩		T_f	N-m		0.16			0.24		0.33
			lb-in		1.4			2.1		2.9
Viscous Damping ①		K_{dv}	N-m/k_{rpm}		0.06			0.13		0.2
			lb-in/k_{rpm}		0.5			1.2		1.8
Thermal Time Constant		TCT	minutes		46			53		60
Thermal Resistance		R_{thw-a}	°C/W		0.43			0.37		0.33
Pole Pairs					5			5		5
Heatsink Size					18"x18"x½" Aluminum Plate			18"x18"x½" Alum. Plate		18"x18"x½" Alum. Plate

Notes:
1. Motor winding temperature rise, ΔT=100°C, at 40°C ambient.
2. All data referenced to sinusoidal commutation.
3. Add parking brake if applicable for total inertia.
4. Motor with standard heatsink.
5. May be limited at some values of Vbus.
6. Measured at 25°C.

7. Brake motor option reduces continuous torque ratings by 1 N-m.
8. Non-Resolver feedback options reduce continuous torque ratings by:
   AKM72 = 2.0 N-m   AKM73 = 2.7 N-m
   AKM74 = 3.4 N-m

9. Motors with non-Resolver feedback and Brake option, reduce continuous torque by:
   AKM72 = 3.9 N-m   AKM73 = 5.1 N-m
   AKM74 = 6.2 N-m
10. For motors with optional shaft seal, reduce torque shown by 0.25 N-m (2.21 lb-in), and increase T_f by the same amount.

Appendix D

Muscle Origin and Insertion

| | | Origin | | | | Insertion | | | |
Muscle	Group	x(cm)	y(cm)	z(cm)		X(cm)	y(cm)	z(cm)	
RFEM	QUAD	-2.4	-4	-1.7	A	0	0	0	C
VASLAT	QUAD	-0.3	-3	-2.2	B	0	0	0	C
VASINT	QUAD	1.7	-14.7	-4	B	0	0	0	C
VASMED	QUAD	-0.3	-9	-4.4	B	0	0	0	C
BIFEMS	HAMS	-0.4	-18.6	-4.1	B	-3.9	1.2	3.1	C
BIFEML	HAMS	-12.1	-9.8	-4.8	A	-3.9	1.2	3.1	C
SEMTEN	HAMS	-12.2	-10	-4.9	A	-2.3	-0.5	-1.9	C
SEMMEM	HAMS	-11	-9.9	-4.4	A	-4.6	1.4	-1.5	C
MEDGAS	CALF	-2	-38	-7.9	B	0.5	0	0.2	D
LATGAS	CALF	-2.6	-39.3	-4.9	B	0.5	0	0.2	D
SOLEUS	CALF	-4.2	-3.2	0.1	C	1	0	0.2	D

Global Reference Frame

	x	y	z
A	3.76	8.78	4.15
B	-5.98	-3.66	5.12
C	1.26	-45.65	5.21
D	10.51	-83.41	6.16

| Global Origin | | | Global Insertion | | | Length | | | | Angle of Line of Action | | |
x(cm)	y(cm)	z(cm)	x(cm)	y(cm)	z(cm)	X(cm)	Y(cm)	Z(cm)	Length	cosX	cosY	cosZ
1.36	4.78	2.45	1.26	-45.65	5.21	0.1	50.43	2.76	50.50557	0.00198	0.998504	0.054647
-6.28	-6.66	2.92	1.26	-45.65	5.21	7.54	38.99	2.29	39.77833	0.18955	0.980182	0.057569
-4.28	-18.36	1.12	1.26	-45.65	5.21	5.54	27.29	4.09	28.1454	0.196835	0.969608	0.145317
-6.28	-12.66	0.72	1.26	-45.65	5.21	7.54	32.99	4.49	34.13725	0.220873	0.966393	0.131528
-6.38	-22.26	1.02	-2.64	-44.45	8.31	3.74	22.19	7.29	23.65434	0.158111	0.938094	0.308189
-8.34	-1.02	-0.65	-2.64	-44.45	8.31	5.7	43.43	8.96	44.70947	0.12749	0.971383	0.200405
-8.44	-1.22	-0.75	-1.04	-46.15	3.31	7.4	44.93	4.06	45.71595	0.161869	0.982808	0.088809
-7.24	-1.12	-0.25	-3.34	-44.25	3.71	3.9	43.13	3.96	43.48665	0.089683	0.991799	0.091062
-7.98	-41.66	-2.78	11.01	-83.41	6.36	18.99	41.75	9.14	46.76775	0.406049	0.892709	0.195434
-8.58	-42.96	0.22	11.01	-83.41	6.36	19.59	40.45	6.14	45.36155	0.431864	0.891724	0.135357
-2.94	-48.85	5.31	11.51	-83.41	6.36	14.45	34.56	1.05	37.47397	0.385601	0.92224	0.028019

Appendix E

Galil Program Array

time step (sec)	A	B	C	D	E	F
0.01	-370.13	0.00	-25.50	0.00	-1160.53	-1280.00
0.02	-234.70	0.00	-84.19	0.00	-477.87	-3840.00
0.03	-206.23	0.00	-161.97	0.00	-1228.80	-6400.00
0.04	-227.77	0.00	-212.67	0.00	-1160.53	-8960.00
0.05	-264.71	0.00	-237.34	0.00	-1024.00	-8465.07
0.06	-286.26	0.00	-268.50	0.00	-887.47	-7304.53
0.07	-286.26	0.00	-297.20	0.00	-1433.60	-6894.93
0.08	-260.86	0.00	-314.37	0.00	-1297.07	-7031.47
0.09	-185.45	0.00	-347.20	0.00	-1365.33	-6553.60
0.1	-100.04	0.00	-371.19	0.00	-1297.07	-7304.53
0.11	-44.09	0.00	-390.08	0.00	-1365.33	-6894.93
0.12	-45.17	0.00	-390.73	0.00	-1297.07	-7031.47
0.13	-71.18	0.00	-372.10	0.00	-682.67	-6894.93
0.14	-73.49	0.00	-357.47	0.00	-1297.07	-6963.20
0.15	-60.25	0.00	-342.94	0.00	-1297.07	-6758.40
0.16	-43.25	0.00	-328.56	0.00	-682.67	-6690.13
0.17	-25.78	0.00	-314.69	0.00	-1297.07	-6485.33
0.18	-8.93	0.00	-302.25	0.00	-614.40	-6280.53
0.19	-3.18	0.00	-277.91	0.00	-614.40	-6144.00
0.2	-0.53	0.00	-253.58	0.00	-614.40	-5966.51
0.21	7.70	0.00	-240.61	0.00	-614.40	-5891.41
0.22	13.62	0.00	-227.13	0.00	-614.40	-5686.61
0.23	20.24	0.00	-217.28	0.00	-614.40	-5666.13
0.24	25.86	0.00	-207.39	0.00	-614.40	-5461.33
0.25	35.32	0.00	-202.38	0.00	0.00	-5393.07
0.26	45.09	0.00	-197.78	0.00	-614.40	-5256.53
0.27	52.63	0.00	-190.05	0.00	0.00	-5188.27
0.28	58.94	0.00	-182.05	0.00	0.00	-5188.27
0.29	64.25	0.00	-175.05	0.00	-750.93	-5051.73
0.3	65.56	0.00	-165.99	0.00	0.00	-5120.00
0.31	76.49	0.00	-172.74	0.00	614.40	-5051.73
0.32	86.18	0.00	-179.35	0.00	-68.27	-5120.00
0.33	91.57	0.00	-180.76	0.00	-68.27	-5051.73
0.34	97.73	0.00	-182.50	0.00	-68.27	-5256.53
0.35	101.57	0.00	-178.85	0.00	614.40	-5324.80
0.36	108.50	0.00	-176.03	0.00	0.00	-5324.80
0.37	110.04	0.00	-162.92	0.00	0.00	-5256.53
0.38	114.66	0.00	-151.56	0.00	819.20	-5393.07
0.39	116.96	0.00	-134.82	0.00	136.53	-5393.07
0.4	118.50	0.00	-118.00	0.00	204.80	-5393.07
0.41	123.12	0.00	-107.61	0.00	955.73	-5529.60
0.42	126.97	0.00	-97.13	0.00	341.33	-5461.33
0.43	126.20	0.00	-81.92	0.00	955.73	-5529.60
0.44	127.74	0.00	-76.91	0.00	1024.00	-5529.60
0.45	135.43	0.00	-75.62	0.00	273.07	-6212.27
0.46	146.21	0.00	-76.12	0.00	1024.00	-5393.07

time step (sec)	A	B	C	D	E	F
0.47	155.44	0.00	-75.11	0.00	955.73	-5393.07
0.48	166.21	0.00	-75.61	0.00	1638.40	-5939.20
0.49	174.68	0.00	-77.77	0.00	1024.00	-5870.93
0.5	180.83	0.00	-80.93	0.00	1024.00	-5188.27
0.51	187.76	0.00	-85.80	-0.36	1092.27	-5734.40
0.52	191.61	0.00	-90.66	-11.58	1160.53	-5734.40
0.53	195.45	0.00	-95.07	-27.42	1911.47	-5734.40
0.54	200.07	0.00	-98.65	-34.99	1228.80	-5666.13
0.55	208.54	0.00	-102.46	-39.83	1365.33	-5666.13
0.56	219.31	0.00	-105.90	-52.15	1433.60	-6280.53
0.57	233.93	0.00	-110.35	-71.08	2252.80	-5597.87
0.58	248.55	0.00	-114.89	-93.69	1570.13	-6212.27
0.59	263.94	0.00	-120.03	-85.85	1638.40	-5529.60
0.6	275.48	0.00	-125.54	-97.85	2389.33	-6075.73
0.61	288.56	0.00	-132.66	-107.54	1843.20	-6007.47
0.62	299.34	0.00	-142.03	-120.93	2389.33	-6485.33
0.63	302.42	0.00	-150.02	-155.08	2048.00	-5734.40
0.64	303.95	0.00	-158.65	-190.62	2048.00	-6144.00
0.65	311.65	0.00	-171.24	-205.85	3413.33	-6007.47
0.66	321.65	0.00	-188.47	-209.54	2048.00	-6348.80
0.67	327.04	0.00	-203.72	-231.70	2730.67	-5461.33
0.68	333.20	0.00	-187.69	-117.23	2048.00	-5802.67
0.69	340.89	0.00	-172.96	-165.00	3413.33	-5461.33
0.7	340.89	0.00	-243.80	-212.77	2730.67	-4846.93
0.71	330.89	0.00	-252.50	-194.31	2730.67	-5461.33
0.72	308.57	0.00	-256.52	-199.85	2730.67	-4096.00
0.73	272.40	0.00	-225.10	-110.77	3413.33	-4096.00
0.74	230.85	0.00	-200.61	-68.77	2730.67	-3413.33
0.75	194.68	0.00	-170.62	-16.62	3413.33	-2730.67
0.76	168.52	0.00	-149.70	0.00	3413.33	-2048.00
0.77	147.74	0.00	-122.93	0.00	2730.67	-1365.33
0.78	145.44	0.00	-106.11	0.00	3413.33	-1365.33
0.79	149.28	0.00	-95.04	0.00	4096.00	0.00
0.8	143.90	0.00	-79.35	0.00	3413.33	682.67
0.81	156.98	0.00	-90.89	0.00	2730.67	1365.33
0.82	136.20	0.00	-67.36	0.00	3413.33	2730.67
0.83	106.19	0.00	-40.78	0.00	3413.33	2048.00
0.84	93.11	0.00	-38.43	0.00	2730.67	4096.00
0.85	86.18	0.00	-42.81	0.00	2048.00	4778.67
0.86	78.49	0.00	-40.88	0.00	2048.00	5461.33
0.87	69.64	0.00	-24.64	0.00	1365.33	6144.00
0.88	60.18	0.00	-28.19	0.00	682.67	6826.67
0.89	52.25	0.00	-18.96	0.00	0.00	6826.67
0.9	47.09	0.00	-10.84	0.00	-682.67	8192.00
0.91	44.71	0.00	0.00	0.00	-2048.00	8874.67

time step (sec)	A	B	C	D	E	F
0.92	44.32	-11.63	0.00	0.00	-2048.00	9557.33
0.93	45.02	-14.58	0.00	0.00	-2730.67	9557.33
0.94	46.09	-21.69	0.00	0.00	-4096.00	10240.00
0.95	47.32	-31.57	0.00	0.00	-3413.33	10922.67
0.96	48.40	-31.06	0.00	0.00	-4096.00	11605.33
0.97	49.09	-29.17	0.00	0.00	-5461.33	11605.33
0.98	48.56	-26.72	0.00	0.00	-4096.00	11605.33
0.99	45.94	-24.46	0.00	0.00	-5461.33	12288.00
1	40.55	-23.03	0.00	0.00	-4778.67	12970.67
1.01	32.32	-22.94	0.00	0.00	-4778.67	13653.33
1.02	21.93	-24.60	0.00	0.00	-5461.33	12970.67
1.03	10.62	-20.77	0.00	0.00	-4096.00	12970.67
1.04	-0.01	-26.81	0.00	0.00	-4778.67	13653.33
1.05	-8.31	-28.29	0.00	0.00	-4096.00	14336.00
1.06	-13.00	-39.87	0.00	0.00	-4778.67	12970.67
1.07	-13.54	-40.24	0.00	0.00	-3413.33	14336.00
1.08	-10.70	-38.03	0.00	0.00	-2730.67	12970.67
1.09	-6.13	-41.44	0.00	0.00	-3413.33	13653.33
1.1	-2.32	-37.70	0.00	0.00	-2048.00	13653.33
1.11	-1.51	-33.23	0.00	0.00	-2730.67	13653.33
1.12	-5.01	-22.98	0.00	0.00	-2048.00	12970.67
1.13	-12.62	-8.26	0.00	0.00	-1365.33	12970.67
1.14	-22.78	-25.66	0.00	0.00	-682.67	8874.67
1.15	-32.93	-8.31	0.00	0.00	-955.73	14336.00
1.16	-41.01	0.00	0.00	0.00	136.53	13653.33
1.17	-46.02	0.00	0.00	0.00	-204.80	12970.67
1.18	-49.02	0.00	0.00	0.00	750.93	6826.67
1.19	-51.79	0.00	0.00	0.00	341.33	6826.67
1.2	-55.79	-4.14	0.00	0.00	1228.80	13653.33
1.21	-61.64	-10.06	0.00	0.00	682.67	6144.00
1.22	-68.79	-19.34	0.00	0.00	1365.33	6144.00
1.23	-76.26	-30.02	0.00	0.00	682.67	6144.00
1.24	-82.34	-23.65	0.00	0.00	3549.87	5051.73

Appendix F

Regression Coefficient Study Graphs

Hamstring Profile

Quadriceps Profile

Calf Profile

Ankle Motion Profile

Hip Motion Profile

Legend: Calculated, Measured, Anybody Model

Y-axis: Joint Motion (m)

X-axis: Time (seconds)
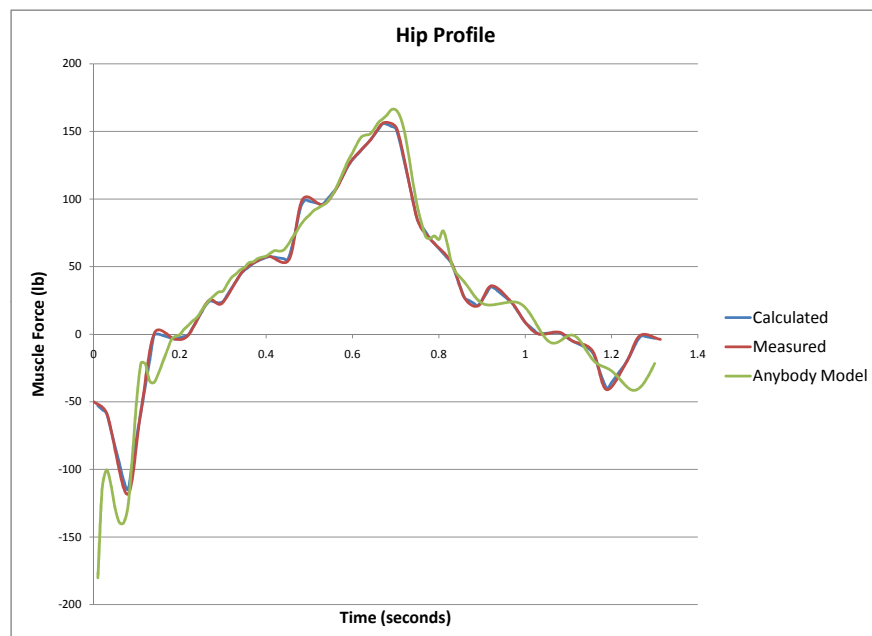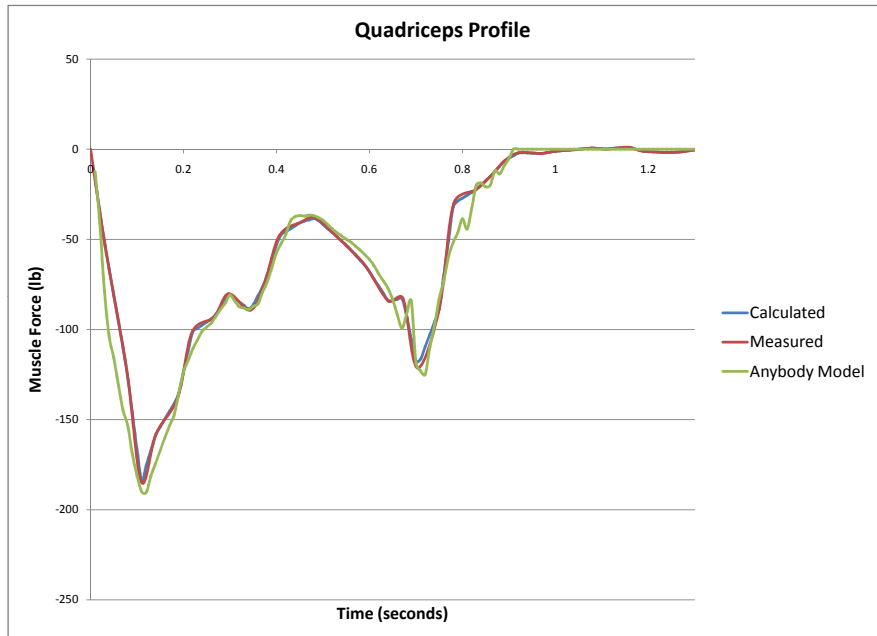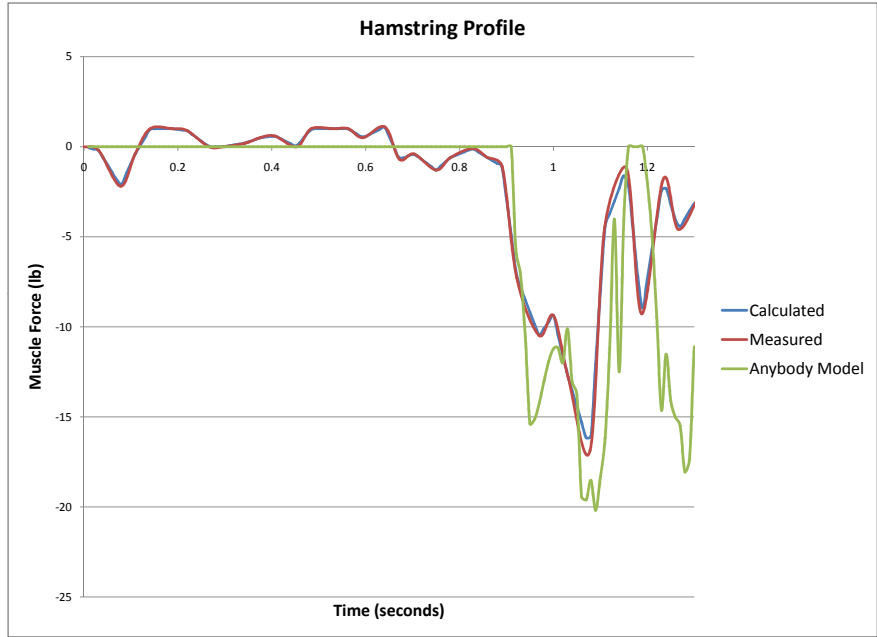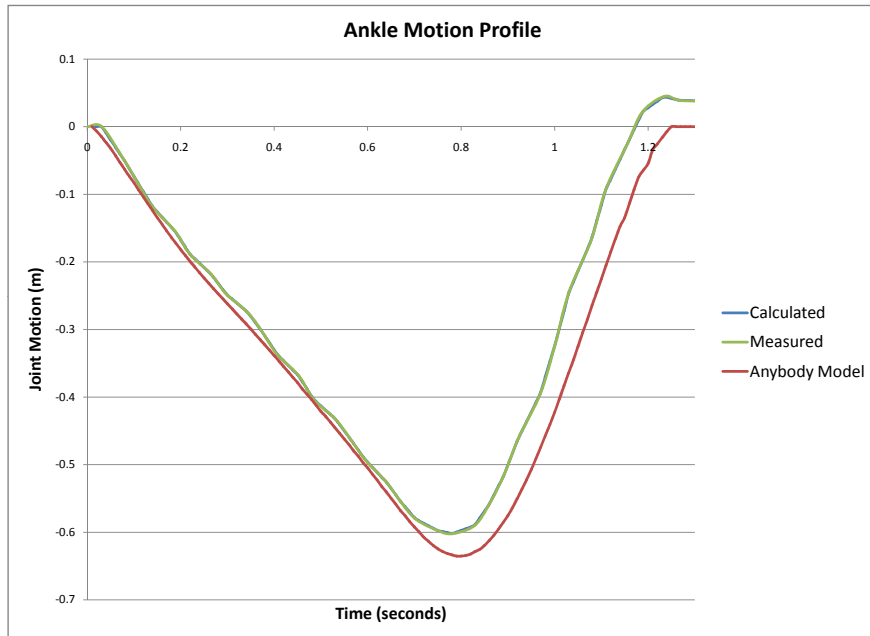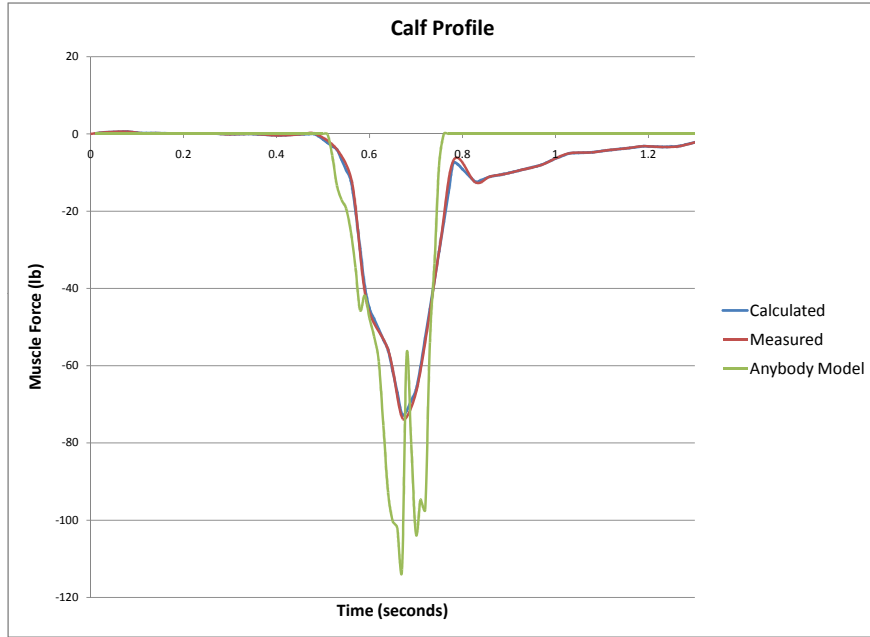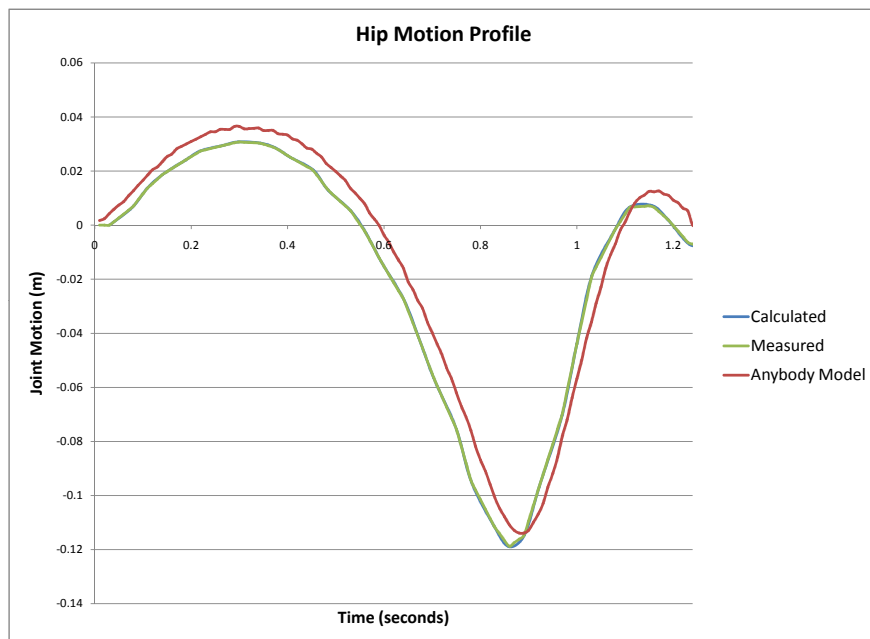
References

[1] http //www.laboratorium.dist.unige.it/p̃iero/teaching/gait/netter/thigh _muscles_superficial_anterior.png. x, 5

[2] http //www.physioweb.org/images/thigh_dorsal.jpg. x, 6

[3] J. Agel, E.A. Arendt, and B. Bershadsky. Anterior cruciate ligament injury in national collegiate athletic association basketball and soccer: a 13-year review. *The American Journal of Sports Medicine*, 33(4):524, 2005. x, 10, 11

[4] E. Arendt and R. Dick. Knee injury patterns among men and women in collegiate basketball and soccer: NCAA data and review of literature. *The American Journal of Sports Medicine*, 23(6):694, 1995. 4, 5, 6

[5] D.R. Bennett, Blackburn T., Boling M.C., McGrath M., Walusz H., and Padua D.A. The relationship between anterior tibial shear force during a jump landing task and quadriceps and hamstring strength. *J. Clin. Biomech.*, 2008. 8, 9

[6] T.B. Birmingham, D.M. Bryant, J.R. Giffin, R.B. Litchfield, J.F. Kramer, A. Donner, and P.J. Fowler. A randomized controlled trial comparing the effectiveness of functional knee brace and neoprene sleeve use after anterior cruciate ligament reconstruction. *The American Journal of Sports Medicine*, 36(4):648, 2008. 53

[7] B.S. Borotikar, R. Newcomer, R. Koppes, and S.G. McLean. Combined effects of fatigue and decision making on female lower limb landing postures: Central and peripheral contributions to ACL injury risk. *Clinical Biomechanics*, 23(1):81–92, 2008. 4

[8] EYS Chao, BA MacWilliams, B. Chan, and L. Meija. Evaluation of a Dynamic Joint Simulator. *Advances in Bioengineering*, 28:281–282, 1994. 15

[9] J.D. Chappell, R.A. Creighton, C. Giuliani, B. Yu, and W.E. Garrett. Kinematics and electromyography of landing preparation in vertical stop-jump: risks for noncontact anterior cruciate ligament injury. *The American Journal of Sports Medicine*, 35(2):235, 2007. 8, 9

[10] J.D. Chappell, B. Yu, D.T. Kirkendall, and W.E. Garrett. A comparison of knee kinetics between male and female recreational athletes in stop-jump tasks. *The American Journal of Sports Medicine*, 30(2):261, 2002. 5, 6, 8, 9

[11] N. Cortes, J. Onate, J. Abrantes, L. Gagen, E. Dowling, and B. Van Lunen. Effects of gender and foot-landing techniques on lower extremity kinematics during drop-jump landings. *Journal of applied biomechanics*, 23(4):289, 2007. 8, 12, 28

[12] M. Damsgaard, J. Rasmussen, S.T. Christensen, E. Surma, and M. de Zee. Analysis of musculoskeletal systems in the AnyBody Modeling System. *Simulation Modelling Practice and Theory*, 14(8):1100–1111, 2006. 1, 14

[13] J.D. DesJardins, P.S. Walker, H. Haider, and J. Perry. The use of a force-controlled dynamic knee simulator to quantify the mechanical performance of total knee replacement designs during functional activity. *Journal of Biomechanics*, 33(10):1231–1242, 2000. 15

[14] DJ DiAngelo and IA Harrington. Design of a dynamic multi-purpose joint simulator. *Adv Bioeng*, 22:107–111, 1992. 15

[15] M. Dienst, G. Schneider, K. Altmeyer, K. Voelkering, T. Georg, B. Kramann, and D. Kohn. Correlation of intercondylar notch cross sections to the ACL size: a high resolution MR tomographic in vivo analysis. *Archives of Orthopaedic and Trauma Surgery*, 127(4):253–260, 2007. 10

[16] Abra Ens. A comparison of gait simulation models in the anybody modeling system. Technical report, University of Waterloo, 2009. 39

[17] B.C. Fleming, P.A. Renstrom, G. Ohlen, R.J. Johnson, G.D. Peura, B.D. Beynnon, and G.J. Badger. The gastrocnemius muscle is an antagonist of the anterior cruciate ligament. *Journal of Orthopaedic Research*, 19(6), 2001. 9

[18] D. Gehring, M. Melnyk, and A. Gollhofer. Gender and fatigue have influence on knee joint control strategies during landing. *Clinical Biomechanics*, 24(1):82–87, 2009. 9

[19] L.Y. Griffin, M.J. Albohm, E.A. Arendt, R. Bahr, B.D. Beynnon, M. DeMaio, R.W. Dick, L. Engebretsen, W.E. Garrett Jr, J.A. Hannafin, et al. Understanding and preventing noncontact anterior cruciate ligament injuries: a review of the Hunt Valley II meeting, January 2005. *The American Journal of Sports Medicine*, 34(9):1512, 2006. 5

[20] J. Hashemi, N. Chandrashekar, T. Jang, F. Karpat, M. Oseto, and S. Ekwaro-Osire. An Alternative Mechanism of Non-contact Anterior Cruciate Ligament Injury During Jump-landing: In-vitro Simulation. *Experimental Mechanics*, 47(3):347–354, 2007. x, 18, 20

[21] G. Hughes and J. Watkins. A Risk-Factor Model for Anterior Cruciate Ligament Injury. *Sports Medicine*, 36(5):411, 2006. x, 4, 5, 6, 7, 8, 9, 10

[22] Arthur F. Dailey Keith L. Moore. *Clinically Oriented Anatomy*. Lippincott Williams & Wilkins, 1999. 1, 2, 5

[23] K. Kiguchi, T. Fukuda, Y. Koga, T. Watanabe, K. Terajima, T. Hayashi, M. Sakamoto, M. Matsueda, Y. Suzuki, and H. Segawa. Development of a physiological knee motion simulator. *Advanced robotics*, 13(2):171–188, 1999. 17

[24] MD Klein Horsman, H. Koopman, FCT van der Helm, L.P. Prosé, and HEJ Veeger. Morphological muscle and joint parameters for musculoskeletal modelling of the lower extremity. *Clinical Biomechanics*, 22(2):239–247, 2007. 40

[25] T. Krosshaug and R. Bahr. A model-based image-matching technique for three-dimensional reconstruction of human motion from uncalibrated video sequences. *Journal of biomechanics*, 38(4):919–929, 2005. 13

[26] T. Krosshaug, JR Slauterbeck, L. Engebretsen, and R. Bahr. Biomechanical analysis of anterior cruciate ligament injury mechanisms: three-dimensional motion reconstruction from video sequences. *Scandinavian Journal of Medicine & Science in Sports*, 17(5):508, 2007. x, 13, 25

[27] L.S. Lohmander, P.M. Englund, L.L. Dahl, and E.M. Roos. The long-term consequence of anterior cruciate ligament and meniscus injuries: osteoarthritis. *The American journal of sports medicine*, 35(10):1756, 2007. 7

[28] LS Lohmander, A. Ostenberg, M. Englund, and H. Roos. High prevalence of knee osteoarthritis, pain, and functional limitations in female soccer players twelve years after anterior cruciate ligament injury. *Arthritis & Rheumatism*, 50(10), 2004. 6, 7

[29] H. Louboutin, R. Debarge, J. Richou, T.A.S. Selmi, S.T. Donell, P. Neyret, and F. Dubrana. Osteoarthritis in patients with anterior cruciate ligament rupture: A review of risk factors. *The Knee*, 2008. 7

[30] L.P. Maletsky and B.M. Hillberry. Simulating dynamic activities using a five-axis knee simulator. *Journal of biomechanical engineering*, 127:123, 2005. 15, 16

[31] K.L. Markolf, D.M. Burchfield, M.M. Shapiro, M.F. Shepard, G.A.M. Finerman, and J.L. Slauterbeck. Combined knee loading states that generate high anterior cruciate ligament forces. *Journal of Orthopaedic Research*, 13(6), 1995. 8

[32] Jackson SR McAllister DR Markolf KL, O'Neill G. Effects of applied quadriceps and hamstrings muscle loads on forces in the anterior and posterior cruciate ligaments. *The American Journal of Sports Medicine*, 32(5):1144–1149, 2004. 9

[33] H.O. Mayr, T.G. Weig, and W. Plitz. Arthrofibrosis following ACL reconstructionreasons and outcome. *Archives of Orthopaedic and Trauma Surgery*, 124(8):518–522, 2004. 7

[34] P. McKinley and A. Pedotti. Motor strategies in landing from a jump: the role of skill in task execution. *Experimental Brain Research*, 90(2):427–440, 1992. 25

[35] CA McLean and AM Ahmed. Design and development of an unconstrained dynamic knee simulator. *Journal of biomechanical engineering*, 115:144, 1993. x, 16, 17

[36] van den Bogert AJ McLean SG, Lipfert SW. Effect of gender and defensive opponent on the biomechanics of sidestep cutting. *Official Journal of the American College of Sports Medicine*, 2004. 5, 7, 12

[37] van den Bogert AJ McLean SG, Su A. Development and validation of a 3-d model to predict knee joint loading during dynamic movement. *Journal of Biomechanical Engineering*, 125:864–874, 2003. 5, 14, 24

[38] Y. Nagano, H. Ida, M. Akai, and T. Fukubayashi. Biomechanical characteristics of the knee joint in female athletes during tasks associated with anterior cruciate ligament injury. *The Knee*, 2008. 12

[39] A. Ortiz, S. Olson, C.L. Libby, E. Trudelle-Jackson, Y.H. Kwon, B. Etnyre, and W. Bartlett. Landing Mechanics Between Noninjured Women and Women With Anterior Cruciate Ligament Reconstruction During 2 Jump Tasks. *The American Journal of Sports Medicine*, 36(1):149, 2008. 7, 12

[40] Torry MR Decker MJ Pandy MG Pflum MA, Shelburne KB. Model prediction of anterior cruciate ligament force during drop-landings. *Official Journal of the American College of Sports Medicine*, 2004. 14, 24

[41] J. Rasmussen, V. Vondrak, Damsgaard, M.M. deZee, and S. Christensen. The Any-Body projectComputer analysis of the human body. *Proceedings of Computer Analysis of the Human Body, Biomechanics of Man*, pages 13–15, 2002. 14

[42] AA Sapega, RA Moyer, C. Schneck, and N. Komalahiranya. Testing for isometry during reconstruction of the anterior cruciate ligament. Anatomical and biomechanical considerations, 1990. 16

[43] Abt JP Sell TC, Ferris CM et al. Predictors of proximal tibia anterior shear force during a vertical stop-jump. *Journal of Orthopaedic Research*, 2007. 5, 8, 9, 12

[44] JA Shaw and DG Murray. Knee joint simulator. *Clinical orthopaedics and related research*, (94):15. 15

[45] Y. Shimokochi and S.J. Shultz. Mechanisms of Noncontact Anterior Cruciate Ligament Injury. *Journal of Athletic Training*, 43(4):396, 2008. 5, 7

[46] S.J. Shultz and A.D. Nguyen. Bilateral Asymmetries in Clinical Measures of Lower-Extremity Anatomic Characteristics. *Clinical Journal of Sport Medicine*, 17(5):357, 2007. 29

[47] J. Susan. *Basic biomechanics*. McGraw Hill Higher Education, 2006. 5

[48] O. Szklar and AM Ahmed. A simple unconstrained dynamic knee simulator. *Journal of biomechanical engineering*, 109(3):247–251, 1987. 16, 19

[49] C.L. Vaughan, B.L. Davis, and C.O.C. Jeremy. *Dynamics of human gait.* Human Kinetics Publishers Champaign, Illinois, 1992. 38, 39, 44

[50] P.S. Weinhold, J.D.N. Stewart, H.Y. Liu, C.F. Lin, W.E. Garrett, and B. Yu. The influence of gender-specific loading patterns of the stop-jump task on anterior cruciate ligament strain. *Injury*, 38(8):973–978, 2007. 48, 50

[51] SC White, HJ Yack, and DA Winter. A three-dimensional musculoskeletal model for gait analysis. Anatomical variability estimates. *Journal of biomechanics*, 22(8-9):885, 1989. 40

[52] D.A. Winter. *The biomechanics and motor control of human gait.* Univ of Waterloo Pr, 1987. 1, 3

[53] T.J. Withrow, L.J. Huston, E.M. Wojtys, and J.A. Ashton-Miller. The effect of an impulsive knee valgus moment on in vitro relative ACL strain during a simulated jump landing. *Clinical Biomechanics*, 21(9):977–983, 2006. x, 8, 19, 20

[54] B. Yu and W.E. Garrett. Mechanisms of non-contact ACL injuries. *British Medical Journal*, 41(Suppl 1):47–51, 2007. 4, 8, 9

[55] B. Yu, C.F. Lin, and W.E. Garrett. Lower extremity biomechanics during the landing of a stop-jump task. *Clinical Biomechanics*, 21(3):297–305, 2006. 8, 9

[56] L.Q. Zhang, J.M. Minorik, F. Lin, J.L. Koh, M. Makhsous, and Z. Bai. ACL strain during simulated free-speed walking. In *Proceedings of the 25th annual meeting of the American Society of Biomechanics. San Diego*, 2001. 48